



**Lehrstuhl für
Technische Dynamik**
Prof. Dr.-Ing. habil. Sigrid Leyendecker

Report

Chair of Applied Dynamics

2016



**FRIEDRICH-ALEXANDER
UNIVERSITÄT
ERLANGEN-NÜRNBERG**
TECHNISCHE FAKULTÄT

© 2016

Prof. Dr.-Ing. habil. S. Leyendecker

Lehrstuhl für Technische Dynamik

Universität Erlangen-Nürnberg

Immerwahrstrasse 1

91058 Erlangen

Tel.: 09131 8561000

Fax.: 09131 8561011

www: <http://www.ltd.tf.uni-erlangen.de>

Editors: N. Kondratieva, M. Eisentraudt

All rights reserved. Without explicit permission of the authors it is not allowed to copy this publication or parts of it, neither by photocopy nor in electronic media.

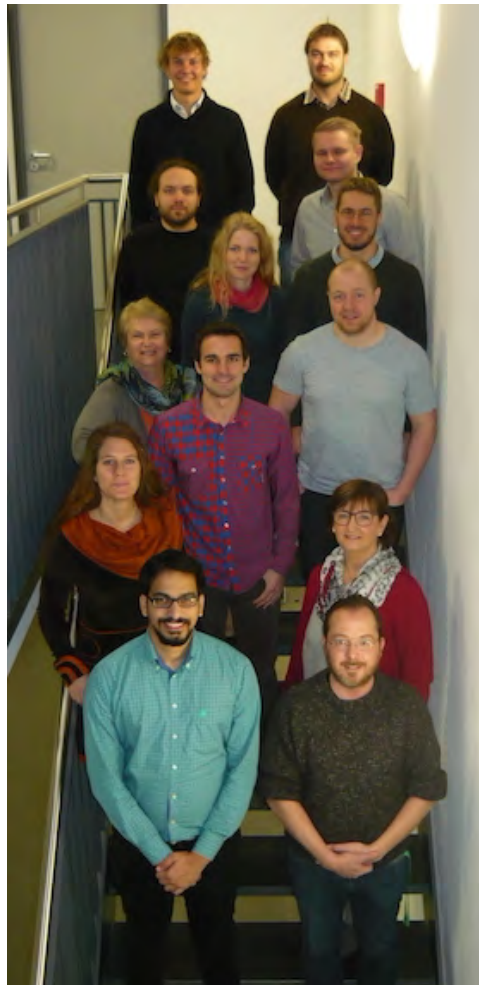
Contents

1	Preface	4
2	Team	5
3	Research	7
3.1	Emmy Noether Independent Junior Research Group	7
3.2	Bionicum	7
3.3	GAMM and GACM	7
3.4	SPP 1886	7
3.5	Cooperation partners	8
3.6	Hardware	8
3.7	Scientific and academic honors	8
3.8	Scientific reports	8
4	Activities	30
4.1	Dynamical laboratory	30
4.2	Teaching	31
4.3	Theses	33
4.4	Seminar for mechanics	34
4.5	Editorial activities	36
4.6	Open day – 50 years Technical Faculty of the FAU Erlangen-Nuremberg	36
4.7	‘MINT Forscherwerkstatt’ 2016 with the START-Foundation	37
5	Publications	38
5.1	Book chapters	38
5.2	Reviewed journal publications	38
5.3	Reviewed proceeding publications	38
5.4	Talks	38
6	Social events	40

1 Preface

This report summarises the activities in research and teaching of the Chair of Applied Dynamics at the University of Erlangen-Nuremberg between January and December 2016. Part of LTD is the Independent Junior Research Group in the DFG Emmy Noether Programme ‘Simulation and optimal control of the dynamics of multibody systems in biomechanics and robotics’ that has been at the University of Kaiserslautern from May 2009 to March 2011.

The main direction of research is computational dynamics and optimal control. Efficient technologies for dynamical and optimal control simulations are developed, facing contemporary life science and engineering problems. The problems under investigation come from biomechanics (natural or impaired human movements and athletic’s high performance, human hand grasping model) and robot dynamics (industrial, spatial and medical) as well as the optimisation and optimal control of their dynamics. Further topics are the modelling and simulation of biological and artificial muscles (as electromechanically coupled problems), multiscale and multirate systems with dynamics on various time scales (examples in astrodynamics as well as on atomistic level), higher order variational integrators, Lie group methods and viscous beam formulations as well as research on structural rigidity and conformational analysis of macromolecules. The development of numerical methods is likewise important as the modelling of the nonlinear systems, whereby the formulation of variational principles plays an important role on the levels of dynamic modeling, optimal control as well as numerical approximation, yielding a holistic approach.



2 Team

chair holder

Prof. Dr.-Ing. habil. Sigrid Leyendecker

technical staff

Beate Hegen

Dipl.-Ing. (FH) Natalia Kondratieva

Sven Lässig

academic scientist

Dr. rer. nat. Holger Lang

postdoc

Dr.-Ing. Ramona Hoffmann

until 31.07.2016

scientific staff

M.Sc. Dominik Budday

M.Sc. Daniel Glaas

Dipl.-Ing. Tobias Gail

Dipl.-Ing. Thomas Leitz

M.Sc. Johann Penner

from 01.12.2016

M.Sc. Uday Phutane

from 01.01.2016

Dipl.-Math. Maik Ringkamp

until 31.12.2016

Dipl.-Ing. Tristan Schlögl

M.Sc. Theresa Wenger

students

Tobias Bader

Dominik Bartels

Daniel Brechter

Lewin Butazzko

Emre Cicek

Simon Dentler

David Elz

Sebastian Falk

Michèle Gleser

Alexander Greiner

Johannes Henneberg

Alexander Hetzner

Johanna Hilsen

Michael Jäger

Simone Kellermann

Ibrahim Kilic

Kilian Kleeberger

Johannes Koch

Björn König

Moritz Manert

Pirmin Molz

Kumar Paras

Johann Penner

Felix Potrykus

Roland Purucker

Uta Rösel

Sebastian Scheiterer

Selina Scherzer

Elisabeth Schmidt

Patrik Steck

Artur Usbek

Sarah Walser

Henrik Wigger

Thomas Will

Jinyu Zhang

Wuyang Zhao

Student assistants are mainly active as tutors for young students in basic and advanced lectures at the Bachelor and Master level. Their contribution to high quality teaching is indispensable, thus financial support from various funding sources is gratefully acknowledged.



B. Hegen



N. Kondratieva



S. Lässig



H. Lang



R. Hoffmann



D. Budday



T. Gail



D. Glaas



T. Leitz



J. Penner



U. Phutane



M. Ringkamp



T. Schlögl



T. Wenger



S. Leyendecker

3 Research

3.1 Emmy Noether Independent Junior Research Group

The Emmy Noether Programme by the German Research Foundation (DFG) supports young researchers in achieving independence at an early stage of their scientific careers. Between May 2009 and March 2011, the Emmy Noether Independent Junior Research Group ‘Simulation and optimal control of the dynamics of multibody systems in biomechanics and robotics’ has been affiliated with the University of Kaiserslautern. The group has been transferred to the University of Erlangen-Nuremberg in April 2011 and has been part of the Chair of Applied Dynamics until the end of 2016. The project resulted in 18 peer-reviewed paper publications, 35 contributions to national and international conferences, three PhD theses (completed in 2014, 2015 and to be completed in 2017) and 6 student theses.

3.2 Bionicum

The Bavarian Environment Agency (LfU) (being the central authority for environmental protection and nature conservation, geology and water resources management) has established the centre for bionics ‘bionicum’ in 2012, consisting of a visitors centre in the Tiergarten of the City of Nuremberg with a permanent exhibition and three research projects with a total financial volume of eight million Euro. One of the projects investigates artificial muscles. The modelling and simulation of the dielectric elastomer actors is developed at the LTD while the Institute for Factory Automation and Production Systems (FAPS) works on the fabrication. To identify material parameters that are necessary for the simulation and optimisation of artificial muscles, a dielectric elastomer test bench is set up at the LTD laboratory. This high voltage test bench allows for measuring artificial muscle forces and strain effects as well as breakdown field strengths. Moreover, electric power supply and control boards for artificial muscles that are developed at the FAPS can be tested and evaluated.

3.3 GAMM and GACM

Sigrid Leyendecker has been elected as an Executive Council Member of the German Association for Computational Mechanics (GACM) for the period of January 2013 to December 2016. The objective of GACM is to stimulate and promote education, research and practice in computational mechanics and computational methods in applied sciences, to foster the interchange of ideas among various fields contributing to computational mechanics, and to provide forums and meetings for the dissemination of knowledge about computational mechanics in Germany.

In February 2014, she has further been elected as a member of the Managing Board of the International Association of Applied Mathematics and Mechanics (GAMM) for two years. GAMM promotes scientific development in all areas of applied mathematics and mechanics, e.g. via the organisation of workshops, in particular for younger scientists, and the international scientific annual GAMM meeting.

3.4 SPP 1886

The German Research Foundation (DFG) has established the Priority Programme ‘Polymorphic uncertainty modelling for the numerical design of structures – SPP 1886’ coordinated by Professor Dr.-Ing. Michael Kaliske from Technische Universität Dresden. Sigrid Leyendecker is part of the programme committee and principal investigator of the project ‘Dynamic analysis of prosthetic structures with polymorphic uncertainty’.

3.5 Cooperation partners

Besides numerous worldwide cooperations with scientists in academia, the LTD is in contact with other institutions and industrial partners. The LTD cooperates with the Fraunhofer Institute for Industrial and Economical Mathematics (ITWM) in Kaiserslautern, Germany on common interests like nonlinear rod dynamics and biomechanics, in particular concerning the development of a human hand model and the simulation of grasping. In this context, we also work together with the Chalmers University of Technology in Gothenburg, Sweden. A cooperation with the Junior research group wearHEALTH and AG Augmented Vision, Department Computer Science, TU Kaiserslautern and German Research Center for Artificial Intelligence (DFKI), aims at bridging the gap between motion capturing and biomechanical optimal control simulations. In collaboration with the Stanford Synchrotron Radiation Lightsource (SSRL) in Palo Alto, California, the LTD does research on structural rigidity and conformational analysis of biomolecules. A strong cooperation on topics ranging from the simulation of multirate dynamics, higher order variational methods to hybrid optimal control problems is going on with the Department of Engineering Science at the University of Oxford, England.

3.6 Hardware

The new Celsius R940 workstation with two Xeon CPUs, NVIDIA Tesla K40 graphic card and Kepler GPU allows the parallel computation of large and complex problems, and the LTD is having a new HP DL380 Gen9 server.

3.7 Scientific and academic honors

For the contribution ‘Dynamic simulation of dielectric elastomer actuated multibody systems’ at the ASME 2016 Conference on Smart Materials, Adaptive Structures and Intelligent Systems (SMASIS), Stowe, VT, USA, 28-30 September, 2016, Tristan Schlögl received the Student Best Paper Award. Tristan Schlögl took the first place for his exercise ‘Übungen zur Dynamik starrer Körper’ in the category ÜP20 as part of the teaching evaluation of the Wintersemester 2015/2016. Holger Lang took the second place for his lecture ‘Mehrkörperdynamik’ in the category VW10 as part of the Teaching Evaluation of the Wintersemester 2015/2016.

3.8 Scientific reports

The following pages present a short overview on ongoing research projects pursued at the Chair of Applied Dynamics. These are partly financed by third-party funding (German Research Foundation (DFG), Bavarian Environment Agency (LfU)) and in addition by the core support of the university.

Research topics

A generalised Fourier method to solve the initial boundary value problem for free vibrating viscoelastic beam models

Holger Lang, Sigrid Leyendecker

On optical data-guided optimal control simulations of human motion

Ramona Hoffmann, Bertram Taetz, Markus Miezal, Gabriele Bleser, Sigrid Leyendecker

Frustration-guided motion planning reveals conformational transitions in proteins

Dominik Budday, Rasmus Fonseca, Sigrid Leyendecker, Henry van den Bedem

Variational multirate integration in multibody dynamics

Tobias Gail, Sina Ober-Blöbaum, Sigrid Leyendecker

Optimal feedback control for constrained mechanical systems

Daniel Glaas, Sigrid Leyendecker

Towards higher order multi-symplectic Lie-group variational integrators for geometrically exact beam dynamics – avoidance of shear locking

Thomas Leitz, Sigrid Leyendecker

Kinematic validation of the human thumb model

Uday D. Phutane, Michael Roller, Staffan Björkenstam, Sigrid Leyendecker

Time transformed mixed integer optimal control problems with impacts

Maik Ringkamp, Sina Ober-Blöbaum, Sigrid Leyendecker

Comparison of finite element models for dielectric elastomers concerning volumetric locking

Tristan Schlögl, Sigrid Leyendecker

Variational integrators of mixed order for systems acting on multiple time scales – The relation of constrained Galerkin variational integrators to Runge-Kutta methods

Theresa Wenger, Sina Ober-Blöbaum, Sigrid Leyendecker

A generalised Fourier method to solve the initial boundary value problem for free vibrating viscoelastic beam models

Holger Lang, Sigrid Leyendecker

Fourier analysis is an extremely powerful and well-established tool for analysing oscillations of undamped linear mechanical structures, especially for beam structures [1, 2]. We extend this method to linear beam structures with viscoelastic damping mechanisms of Kelvin-Voigt kind, where the viscous stress contribution is proportional to the strain rate. In the following, we sketch the proposed generalised Fourier method.

The dynamic motion of a homogeneous and uniform axial beam with Kelvin-Voigt viscoelasticity can be described by its **normal displacement** $u(x, t)$, a real valued scalar function of the undeformed arclength parameter $0 \leq x \leq 1$ and the time $t \in \mathbb{R}$. The equation of motion can be formulated as

$$\ddot{u} = u'' + 2\zeta\dot{u}', \quad \text{where } 0 \leq x \leq 1, \quad t \in \mathbb{R} \quad (1)$$

with the **viscosity** $\zeta \geq 0$. Here, $' = \partial/\partial x$ and $\dot{} = \partial/\partial t$. For a derivation of (1), which is formulated in non-dimensional form, see [4]. The internal **normal force** (or normal stress in the non-dimensional setting) is given by $N = u' + 2\zeta\dot{u}'$, where u' is the normal strain and \dot{u}' is its rate. We impose the following initial resp. boundary conditions

$$u(x, 0) = u_0(x), \quad \dot{u}(x, 0) = \dot{u}_0(x) \quad \text{resp.} \quad u(0, t) \equiv 0, \quad u'(1, t) \equiv 0, \quad (2)$$

where $0 \leq t$ and $0 < x < 1$. In (2), the initial positions $u_0(x)$ and initial velocities $\dot{u}_0(x)$ are prescribed functions of x . The boundary conditions in (2) belong to those of a cantilever. Note that $u'(1, t) \equiv 0$ implies $\dot{u}'(1, t) \equiv 0$. Therefore, the normal force at the right free end vanishes identically, i.e. $N(1, t) \equiv 0$.

As demonstrated in [3], it is straightforward to see that real eigensolutions of (1), subjected to the boundary conditions (2), take the form

$$u_n(x, t) = f_n(t)U_n(x), \quad \text{where } U_n(x) = \sqrt{2} \sin(\omega_n x), \quad \omega_n = \left(n + \frac{1}{2}\right)\pi \quad (3)$$

and

$$f_n(t) = \exp(-\omega_n^2 \zeta t) \begin{cases} a_n \cos(\omega_n \sqrt{1 - \omega_n^2 \zeta^2} t) + b_n \sin(\omega_n \sqrt{1 - \omega_n^2 \zeta^2} t) & \text{if } \zeta < 1/\omega_n \\ a_n + b_n t & \text{if } \zeta = 1/\omega_n \\ a_n \exp(\omega_n \sqrt{\omega_n^2 \zeta^2 - 1} t) + b_n \exp(-\omega_n \sqrt{\omega_n^2 \zeta^2 - 1} t) & \text{if } \zeta > 1/\omega_n \end{cases} \quad (4)$$

for each $n = 0, 1, 2, \dots$. In (3), the number ω_n denotes the n -th **undamped eigenfrequency**. Its corresponding **mode shape function** is $U_n(x)$, see [1]. The reciprocal $1/\omega_n$ is the **critical viscosity** of the n -th eigenmode of the beam, the **total critical viscosity** ζ^* is defined as the critical viscosity for the zeroth eigenmode, i.e. $\zeta^* = 1/\omega_0 = 2/\pi$, see [3, 4].

We assume, that the solution $u(x, t)$ in (1) with (2) can be expanded into a **generalised Fourier series** of the form

$$u(x, t) = \sum_{n=0}^{\infty} f_n(t)U_n(x). \quad (5)$$

We let $\langle v, w \rangle = \int_0^1 v(x)w(x) dx$ for square integrable functions $v = v(x)$ and $w = w(x)$ on $[0, 1]$. Due to the orthonormality relationship $\langle U_n, U_m \rangle = \delta_{nm}$ for $n, m = 0, 1, 2, \dots$, the well-known Fourier expansions $u_0(x) = \sum_{n=0}^{\infty} \langle U_n, u_0 \rangle U_n(x)$ and $\dot{u}_0(x) = \sum_{n=0}^{\infty} \langle U_n, \dot{u}_0 \rangle U_n(x)$ hold on $[0, 1]$. Now, if (5) holds, it can be shown that the Fourier coefficients a_n and b_n in (4) must take the following forms.

If $\zeta < 1/\omega_n$,

$$a_n = \langle U_n, u_0 \rangle, \quad b_n = \frac{1}{\omega_n} \left(\langle U_n, \dot{u}_0 \rangle + a_n \omega_n^2 \zeta \right) \sqrt{1 - \omega_n^2 \zeta^2}. \quad (6)$$

If $\zeta = 1/\omega_n$,

$$a_n = \langle U_n, u_0 \rangle, \quad b_n = \langle U_n, \dot{u}_0 \rangle + a_n \omega_n^2 \zeta. \quad (7)$$

If $\zeta > 1/\omega_n$,

$$\begin{aligned} a_n &= \frac{1}{2\omega_n \sqrt{\omega_n^2 \zeta^2 - 1}} \left[\omega_n \left(\sqrt{\omega_n^2 \zeta^2 - 1} + \omega_n \zeta \right) \langle U_n, u_0 \rangle + \langle U_n, \dot{u}_0 \rangle \right] \\ b_n &= \frac{1}{2\omega_n \sqrt{\omega_n^2 \zeta^2 - 1}} \left[\omega_n \left(\sqrt{\omega_n^2 \zeta^2 - 1} - \omega_n \zeta \right) \langle U_n, u_0 \rangle - \langle U_n, \dot{u}_0 \rangle \right]. \end{aligned} \quad (8)$$

Example We consider the initial data $u_0(x) = x$ and $\dot{u}_0(x) = 0$, where $0 < x < 1$. Then, we have $\langle U_n, u_0 \rangle = 4\sqrt{2}(-1)^n/\pi^2/(2n+1)^2$ and $\langle U_n, \dot{u}_0 \rangle = 0$ for $n = 0, 1, 2, \dots$ by induction, similarly derived as in [2]. Figure 1 displays the Fourier resp. Finite Element solution for a sufficiently large number of elements. Both agree, which indicates the validity of the proposed method.

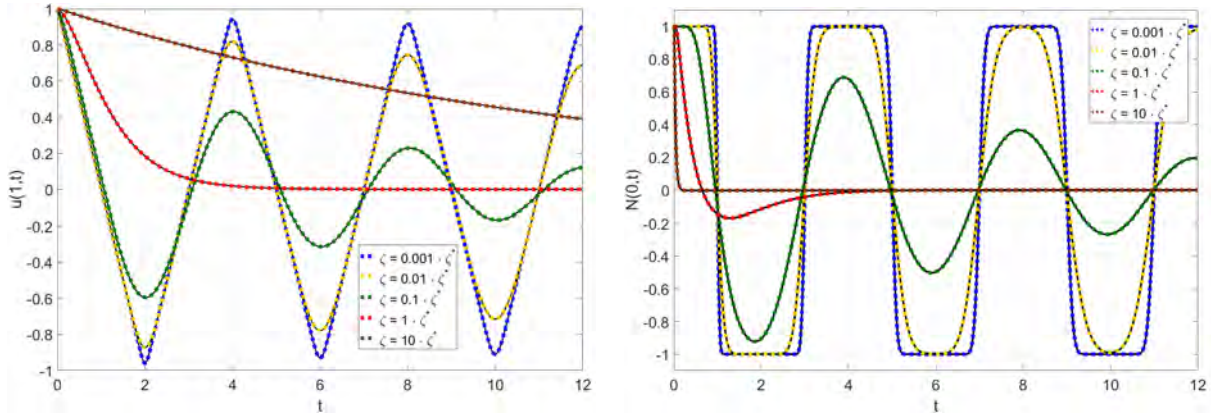


Figure 1: Solution of the IVBP (1), (2). Left: Displacement $u(1, t)$. Right: Normal force $N(0, t)$. Colored: Fourier solution according to (5) together with (6), (7) and (8). Black: Finite Element solution according to [4, 5]

The extension of the proposed Fourier method to bending beams of Kelvin-Voigt type, convergence issues and the quantitative contribution of each $u_n(x, t)$ to (5) are topics of future research.

References

- [1] R.R. Craig and A.J. Kurdila. *Fundamentals of structural mechanics*. John Wiley & Sons, 2006.
- [2] H. Heuser. *Funktionalanalysis*. Teubner, 1998.
- [3] H. Lang, S. Leyendecker, and J. Linn. *Numerical experiments for viscoelastic Cosserat rods with Kelvin-Voigt damping*. Proceedings of the ECCOMAS Thematic Conference on Multibody Dynamics, pp. 453-462, July 1-4, Zagreb, Croatia, 2013.
- [4] H. Lang and S. Leyendecker. *Complex frequency response for linear beams with Kelvin-Voigt viscoelastic material*. Proceedings of the 4th Joint International Conference on Multibody System Dynamics, pp. 282-301, May 29-June 2, Montréal, Canada, 2016.
- [5] H.R. Schwarz. *Finite element methods*. Teubner, 1991.

On optical data-guided optimal control simulations of human motion

Ramona Hoffmann, Bertram Taetz¹, Markus Miezal¹, Gabriele Bleser¹, Sigrid Leyendecker

This work addresses the synergistic fusion of optimal control simulations and marker-based optical measurements of human motion. The latter is a widespread capturing technology in biomechanics and movement science [1]. In the context of optimal control simulations using DMOCC [2], the idea is to improve the computational performance by using a realistic initial guess and to increase the realism of the simulated motion through data-guiding. In the context of motion capturing, the idea is to use biomechanical simulations in order to maintain accurate capturings also with reduced measurement frequencies and points. This would greatly improve the usability of such systems in terms of setup time and wearing comfort. In this work, we investigate different methods for combining physical laws, 3D marker positions obtained from the optical system, and physiologically motivated objectives in an optimal control framework. Moreover, we explore the potential of obtaining reasonable results — in terms of motion trajectories and torques that are close to reference obtained from using all available information — with a reduced measurement frequency and a reduced number of markers. As an extension to our previous work [3], the tests are performed on a human steering and throwing motion, where a human arm was captured with seven retroreflective markers at 120 Hz. We consider two specific scenarios: a steering manoeuvre as a short and slow motion and a faster, more complex and far reaching motion, i.e. a throwing motion. Based on these scenarios, we investigate in particular the following aspects:

- I. How should the measured marker positions be incorporated into the optimisation, i.e., in the objective function as so called soft constraints or as hard constraints to the optimisation?
- II. What are the effects of a reduced measurement update rate or a reduced number of marker points used in the optimal control simulation, how are these effects attenuated by combining the measurements with a physiologically motivated cost function and which function would be best suited? Effects refer here to the deviation of the simulated motion and torques from the simulation results when using all available measurements.

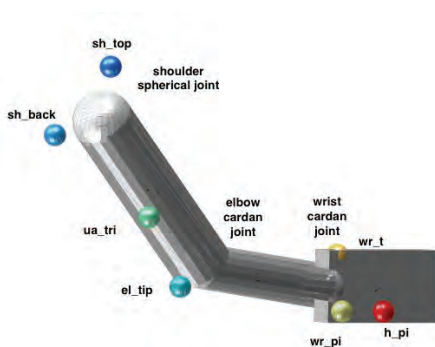


Figure 1: Human arm model with marker positions used for optimal control simulations. The marker labels are introduced in Figure 2

Human arm model and measurement For the simulation, the human arm is modelled as a multi-body system consisting of three rigid bodies. A cylindrical upper arm is fixed in space by a spherical joint representing the shoulder. The elbow and wrist are modelled as cardan joints connecting the cylindrical forearm to the upper arm and the parallelepiped shaped hand to the forearm, respectively (cf. Figure 1). The bodies' dimensions and rotation axes are personalised for the subject and the optical marker positions, relative to the arm segments, are computed from the measurement data via an inverse kinematics optimisation. Thus, the exact definition of the personalised model is already a result from the measured data.

¹Junior research group wearHEALTH, Department Computer Science, University of Kaiserslautern, Germany

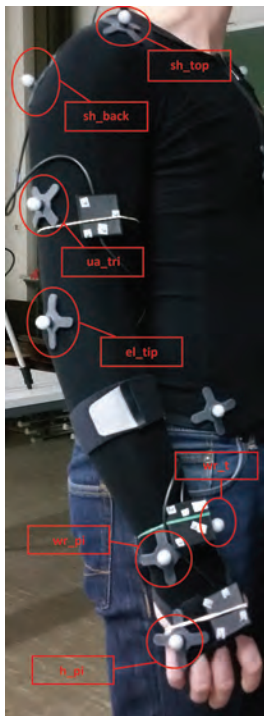


Figure 2: Measurement setup and optical marker protocol with marker labels. Note, for future experiments, we also captured inertial measurements at 120 Hz from three inertial measurement units (IMUs) attached to the upper-, forearm and hand. These IMUs, which are mounted in special casings with tiny markers on top, are also visible in the figure, however, the data is not used in the present study.

Results and discussion Concerning the question (I), the inclusion of the measurements as soft constraints by minimising the residual total deviation between measured and simulated marker positions in the objective function turns out to be computationally way more inefficient than their inclusion as hard constraints. Also, considering that it is a priori known that there are differences between the real motion, the measurement (having errors including those due to soft tissue artefacts) and the simulation (model assumptions on morphology, physiology and actuation as well as discretisation errors), indicates that — instead of using the soft constraints approach — it is more promising to use the measurements as guiding points and to define an environment around them, where a solution of a biomechanical simulation with a physiologically motivated objective criterion is to be found.

Addressing aspect (II), from the investigated objective functions in the steering example, minimising torque change shows the most realistic and natural results and the highest stability with respect to the reduction of the measurement frequency. The second example investigates a throwing motion, which is a far reaching and fast motion compared to the steering motion investigated before. Here, neglecting markers leads to a larger number of failed simulations.

Our results show, that a significant reduction of exploited measurements still provides feasible simulation results in our proposed method, given that the physiologically motivated objective reflects the actual movement. Further, it turns out that neglecting markers close to the shoulder has less influence on the simulation results than neglecting markers close to the hand.

References

- [1] G. Bleser, D. Damen, A. Behera, G. Hendeby, K. Mura, M. Miezal, et al. *Cognitive learning, monitoring and assistance of industrial workflows using egocentric sensor networks*. PLoS ONE, Vol. 10, No. 6, 2015.
- [2] S. Leyendecker, S. Ober-Blöbaum, J. Marsden, and M. Ortiz. *Discrete mechanics and optimal control for constrained systems*. Optimal Control Applications & Methods, Vol. 31, No. 6, pp. 505-528, 2010.
- [3] T. Gail, R. Hoffmann, M. Miezal, G. Bleser, and S. Leyendecker. *Towards bridging the gap between motion capturing and biomechanical optimal control simulations*. Proceedings of the Multibody Dynamics ECCOMAS Thematic conference, 10 pages, Barcelona, Spain, 2015.

Frustration-guided motion planning reveals conformational transitions in proteins

Dominik Budday, Rasmus Fonseca², Sigrid Leyendecker, Henry van den Bedem³

Alternative, non-native contacts play a critical role in conformational dynamics by stabilizing native states and redirecting collective motions, embodied by the principle of minimal frustration. However, frustration also severely hinders fast exploration of conformational space. Here, we exploit frustration to guide conformational transitions by introducing dynamic, Clash-avoiding Constraints (dCC) in a bidirectional, rapidly-exploring random tree (RRT), which allows us to identify transitions between states across scales, from individual side-chains to large multi-domain proteins. Simulating how proteins transition between substates will help us understand the molecular mechanisms of function [1].

We coupled dCC-RRT to our kino-geometric sampler (KGS), which encodes a protein as a kinematic linkage with backbone and side-chain dihedral angles as degrees of freedom [2, 3]. Non-covalent hydrogen bonds and non-native contacts constitute a dynamic set of holonomic constraints that require collective motions of the degrees of freedom, which we compute directly in the constraint manifold. Whenever two atoms are in close contact, we introduce a temporary, interatomic constraint that lets atoms slide past each other (<http://bit.ly/1WZxhcJ>). The new constraint instantaneously alters the constraint manifold, redirecting collective motions to navigate the rugged energy landscape (Fig. 1 left). While linkages with few degrees of freedom would suffer almost direct immobility with this procedure, the high dimensional conformation space of a protein can accommodate a number of clash-constraints and still be moveable. We augmented a bidirectional RRT [4] growing from an initial and a target conformation to connect both states with iteratively updated subsets we call moving fronts (mf) to efficiently select samples during exploration.

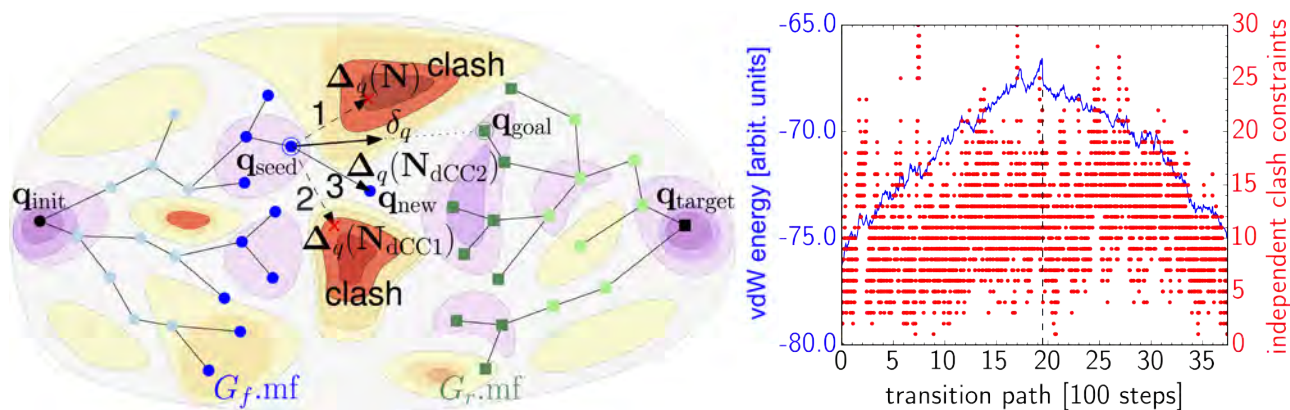


Figure 1: dCC-RRT navigates a rugged energy landscape (left) to connect an initial and a target state by introducing dynamic, Clash-avoiding Constraints (dCC). Clash constraints maintain favorable energies during the transition (right).

We first applied dCC-RRT to a test set of eight proteins with, on average, 7.5Å heavy-atom root mean squared distance (RMSD) between their two substates. Our clash-free pathways reduced the heavy-atom RMSD by 72% on average, outperforming peer methods. Clash constraints ensured favorable energy levels throughout the transition (Fig. 1 right), while a remaining energy barrier reflected the remaining distance between the two closest identified conformations. We then applied dCC-RRT to human cyclophilin A (cypA), whose active site conformational changes are characterized by small-scale changes of side-chains [5, 6], out of range for other, less detailed methods. We found that areas

²Department of Molecular and Cellular Physiology, Stanford University, California, Menlo Park, USA

³Division of Biosciences, SLAC National Accelerator Laboratory, Stanford University, California, Menlo Park, USA

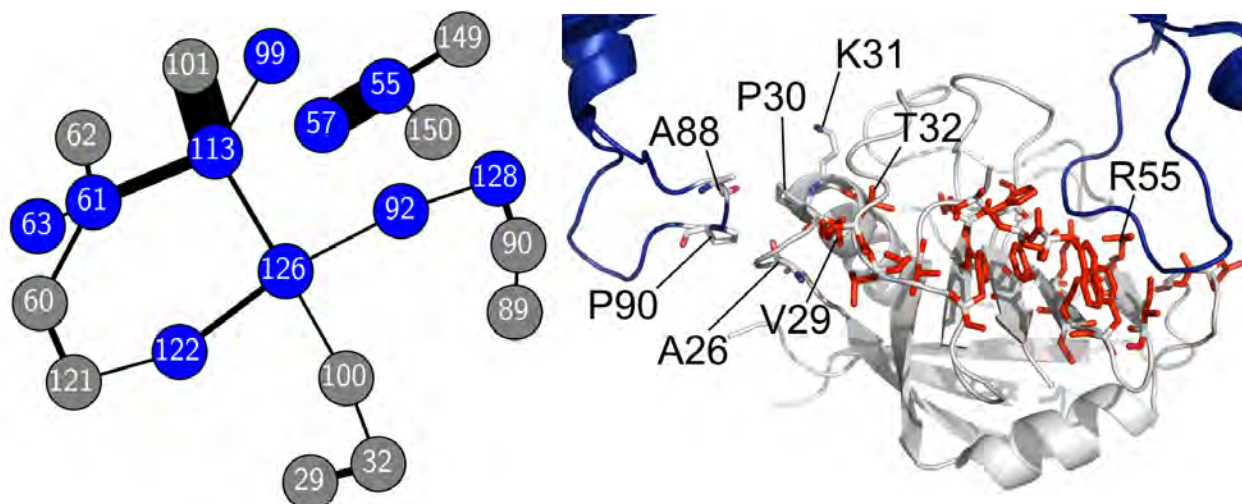


Figure 2: Residue network (graphs left, red residues right) in cypA, connecting the active site at R55 to a second, non-canonical binding site 25 Å away. Blue-colored nodes show similar exchange rates in CPMG experiments⁶. Gray nodes: no exchange measured.

enriched in non-native contacts in dCC-RRT transition pathways form a previously uncharacterized, spatially contiguous network of residues (Fig. 2). Strikingly, the network connects the active site of cypA to a recently proposed, non-canonical capsid binding site 25 Å away [7]. Our network extends and agrees with those we found using multi-temperature crystallography [6] and provides a structural basis for CPMG data [8], validating the ability of dCC-RRT to reveal detailed, all-atom molecular mechanisms for small and large amplitude motions.

References

- [1] H. van den Bedem and J.S. Fraser. *Integrative, dynamic structural biology at atomic resolution – it's about time*. Nat. Meth., Vol. 12, pp. 307-318, 2015.
- [2] D. Budday, S. Leyendecker, and H. van den Bedem. *Geometric analysis characterizes molecular rigidity in generic and non-generic protein configurations*. Journal of the Mechanics and Physics of Solids, Vol. 83, pp. 36-47, 2015.
- [3] D.V. Pachov, R. Fonseca, D. Arnol, J. Bernauer, and H. van den Bedem. *Coupled motions in β 2AR: $G\alpha$ s conformational ensembles*. J. Chem. Theory Comput., Vol. 12, pp. 946-956, 2016.
- [4] J. Kuffner and S. Lavallo. *RRT-connect: An efficient approach to single-query path planning*. Robotics and Automation, ICRA'00 IEEE International Conference, 2000.
- [5] J.S. Fraser, M.W. Clarkson, S.C. Degnan, R. Erion, Renske D. Kern, and T. Alber. *Hidden alternative structures of proline isomerase essential for catalysis*. Nature, Vol. 462, pp. 669-673, 2009.
- [6] D.A. Keedy et al. *Mapping the conformational landscape of a dynamic enzyme by multitemperature and XFEL crystallography*. eLife, Vol. 4, pp. e07574, 2015.
- [7] C. Liu et al. *Cyclophilin A stabilizes the HIV-1 capsid through a novel non-canonical binding site*. Nat. Commun., Vol. 7, pp. 10714, 2016.
- [8] J. Schlegel, G.S. Armstrong, J.S. Redzic, F. Zhang, and E.Z. Eisenmesser. *Characterizing and controlling the inherent dynamics of cyclophilin-A*. Protein Sci., Vol. 18, pp. 811-824, 2009.

Variational multirate integration in multibody dynamics

Tobias Gail, Sina Ober-Blöbaum¹, Sigrid Leyendecker

Mechanical systems with dynamics on different time scales have contradicting requirements on the integration method. On the one hand, for stable integration of the fast dynamics, tiny time step sizes are needed. On the other hand, for the slow dynamics, large time steps are accurate enough. Both demands are fulfilled in the framework known as variational multirate integration [2], where two time grids are used, to integrate the system's dynamics. Here, we focus on the simulation of rigid multi-body systems with dynamics on different time scales. The description of the rigid body uses the so called director formulation [1]. The rigid bodies are connected with joints described by holonomic constraints which have to be considered on different time scales, because they connect bodies with dynamics on different time scales. A variation of the null space method for multirate integration is introduced and the effect on the number of unknowns is investigated.

Let a mechanical system containing slow and fast dynamics be described by a Lagrangian with configuration vector $q \in Q$ with Q a manifold and velocity vector $\dot{q} \in T_q Q$ being in the tangent space $T_q Q$ at q . The motion is constrained by the m -dimensional vector valued function of holonomic, skleronomic constraints requiring $g(q) = 0$. To model the slow and fast dynamics, we split the configuration into n^s slow variables q^s and n^f fast variables q^f and split the potential energy into a slow potential $V(q)$ and a fast potential $W(q^f)$. The action is the time integral of the Lagrangian consisting of the difference of the kinetic energy T and the split potential $V + W$ and the constraints times the Lagrange multipliers λ . Via Hamilton's principle requiring stationarity of the action, the constrained multirate Euler-Lagrange equations are derived.

$$\frac{d}{dt} \frac{\partial T}{\partial \dot{q}^s} + \frac{\partial V}{\partial q^s} - \left(\frac{\partial g}{\partial q^s} \right)^T \cdot \lambda = 0 \quad \frac{d}{dt} \frac{\partial T}{\partial \dot{q}^f} + \frac{\partial V}{\partial q^f} + \frac{\partial W}{\partial q^f} - \left(\frac{\partial g}{\partial q^f} \right)^T \cdot \lambda = 0 \quad g(q) = 0 \quad (1)$$

In the discrete setting, we introduce two time grids, a macro grid with the macro time step ΔT and a micro grid with the micro time step Δt , see Figure 1. The slow variables live on the macro time grid, the fast variables on the micro time grid, and the Lagrange multipliers on both time grids. The action in one macro time interval is approximated by the discrete Lagrangian and discrete constraints. The action sum over all time steps approximates the action integral. Via a discrete form of Hamilton's principle, the discrete constrained variational multirate Euler-Lagrange equations are derived.

In the director formulation, the position of the mass middle point of the rigid body is denoted by the vector $\varphi \in R^3$. The rotational degrees of freedom are described by an orthonormal vector triad, the so called directors $d_I \in R^3$ with $I = 1, 2, 3$. Then, the position and orientation of the rigid body are $q = [\varphi, d_1, d_2, d_3]^T$. The configuration of each body belongs either to the slow or to the fast part of the configuration vector. The directors give rise to six so called internal constraints $g_{int}(q) = 0$ which ensure the orthonormality of the director triad. The rigid bodies are connected by joints, they are described by the vector valued function of the external constraints $g_{ext}(q) = 0$. The constraints of the system then are $g(q) = [g_{int}(q), g_{ext}(q)]^T$. The constraints can be distinguished into purely slow, coupling (slow-fast), and purely fast constraints $g = [g^s, g^{sf}, g^f]^T$. Then, the number of constraints

¹Department of Engineering Science, University of Oxford, England

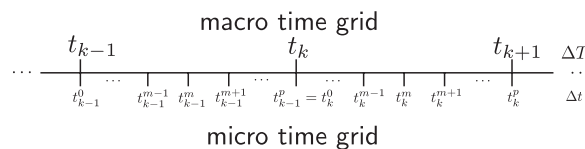


Figure 1: Macro and micro time grid with p micro intervals per macro interval

Δt fixed		Lagrange multiplier method	null space method
$[0 \Delta t]$	$p = 1$	$n^s + n^f + m^s + m^{sf} + m^f$	$n^s + n^f + m^{sf}$
$[0 p\Delta t]$	$p > 1$	$n^s + m^s + p(n^f + m^{sf} + m^f)$	$n^s + p(n^f + m^{sf})$
$[0 t_N]$	$p > 1$	$\frac{t_N}{\Delta t} \left(\frac{1}{p} (n^s + m^s) + (n^f + m^{sf} + m^f) \right)$	$\frac{t_N}{\Delta t} \left(\frac{1}{p} n^s + (n^f + m^{sf}) \right)$

Table 1: Number of unknowns

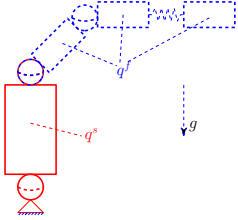


Figure 2: Chain of four rigid bodies

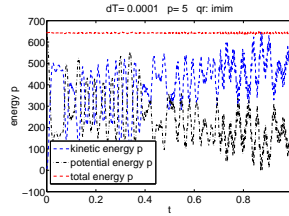


Figure 3: Energy versus time

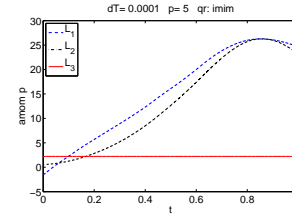


Figure 4: Angular momentum versus time

m can be split into $m = m^s + m^{sf} + m^f$ with m^s the dimension of the slow, m^{sf} of the coupling and m^f of the fast constraints. Due to the presence of λ in (1), the number of unknowns in the system is great than the degrees of freedom of the system. To decrease the number of unknowns, a projection with a so called null space matrix $P(q)$ is performed where $G(q) \cdot P(q) = 0$ with $G = \frac{\partial g(q)}{\partial q}$. The null space matrix can be partitioned to eliminate only certain constraint forces $G^T \cdot \lambda$. Here, the purely slow constraint forces $G^s \cdot \lambda^s$ and purely fast constraint forces $G^f \cdot \lambda^f$ are eliminated. Then, for this null space matrix $P^T \cdot \begin{bmatrix} G^{sT} & G^{sfT} & G^{fT} \end{bmatrix} = \begin{bmatrix} 0 & \overline{G}^{sfT} & 0 \end{bmatrix}$ holds.

With t_N the end time of a simulation, the number of macro time steps is $N = t_N/p\Delta t$ where p is the number of micro steps per macro step. We compare the number of unknowns for one macro time step $[0, \Delta T]$ and for the whole simulation $[0, t_N]$. In Table 1, the number of unknowns are displayed for the single rate ($p = 1$) and multirate ($p > 1$) case for the Lagrange multipliers method and the null space method. From the table it can be seen that the number of unknowns increases when going from single rate in $[0\Delta t]$ to multirate simulation for $[0p\Delta t]$. However, for the whole simulation to t_N the number of all unknowns is reduced in the multirate case compared to the single rate case. In all cases, the null space technique reduces the number of unknowns.

A multi-body system which consists of four bodies connected by spherical joints, see Figure 2, is simulated with the variational multirate integration. The first large and heavy body moves slowly while the other three small bodies are fast. Between the last two bodies, there is a spring with a fast potential W and the slow energy is the potential energy. For a simulation with $\Delta T = 0.0001$, $t_n = 1$ and $p = 5$, Figure 3 shows the good energy behaviour and the preservation of the angular momentum component in gravity direction is illustrated in Figure 4.

References

- [1] P. Betsch, and S. Leyendecker. *The discrete null space method for the energy consistent integration of constrained mechanical system. Part II: Multibody dynamics*. Int. J. Numer. Meth. Engng. Vol. 67, pp. 499-552, 2006.
- [2] S. Leyendecker, S. Ober-Blöbaum. *A variational approach to multirate integration for constrained systems*. Multibody Dynamics, Computational Methods in Applied Sciences, Computational Methods in Applied Sciences, J. C. Samin, P. Fiset (eds.), pp. 97-121, Springer, 2013.

Optimal feedback control for constrained mechanical systems

Daniel Glaas, Sigrid Leyendecker

When doing optimal control one wants to combine the offline optimisation of a desired trajectory with an online feedback control to eliminate perturbations from the optimal trajectory. In the simulation here, the variational integrator as a variant of a structure-preserving integration scheme is used. A midpoint quadrature rule is used to approximate the action in one time interval via a discrete Lagrangian $L_d(q_k, q_{k+1}) \approx \int_{t_k}^{t_{k+1}} L(q(s), \dot{q}(s)) ds$ with configuration sequence $q_k \approx q(t_k)$ for $k = 0, \dots, N$. Applying a discrete variational principle $\delta S_d(\{q_k\}_{k=0}^N) = 0$, see [3], and an approximation of the virtual work $F_d^\pm(q_k, q_{k+1}, u_k)$ with control sequence $\{u_k\}_{k=0}^{N-1}$, the Lagrange-d'Alembert principle yields a discrete Euler-Lagrange equation in a "position-momentum form that only depends on the current and future time steps" [2]. This principle is applied to three different coordinate choices, see Table 1. In redundant coordinates the movement is forced to the manifold by using holonomic constraints $g(q(t)) = 0$, $G(q_k) = \frac{\partial g(q_k)}{\partial q_k}$ and a nullspace matrix $P(q_k)$ with $P^T(q_k) \cdot G^T(q_k) = 0$. To compute the desired trajectory, initial and final conditions on the configuration and conjugate momentum together with the discrete equations in minimal coordinates (see Table 1) serve as non-linear equality constraints for the minimisation of a given objective functional. Applying the DMOC (discrete mechanics and optimal control [4]) algorithm, an optimal trajectory and according control input is calculated.

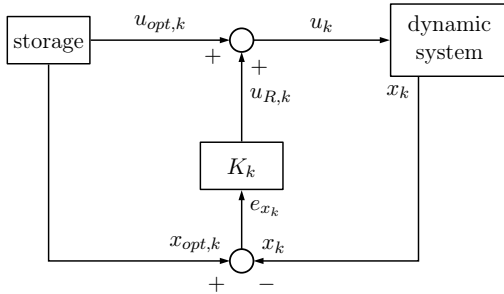


Figure 1: Block diagram of general feedback control

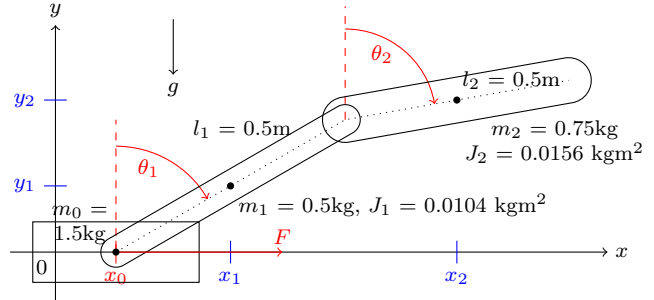


Figure 2: Sketch of the rigid body double pendulum on a cart

The correction of perturbations is done by a feedback controller. An additional control value $u_{R,k}$ is added to the optimal control input $u_k = u_{opt,k} + u_{R,k}$. It is calculated by $u_{R,k} = K_k e_{x_k}$, which is a multiplication of a feedback matrix K_k with the error $e_{x_k} = x_{opt,k} - x_k$, being the difference between desired x_{opt} and "measured" state x . Figure 1 shows the resulting block structure. In the context of the optimal control approach, the Riccati feedback controller is commonly used to minimise a cost-function $V = \sum_{k=0}^{N-1} [e_{x_k}^T Q_k e_{x_k} + u_{R,k}^T R_k u_{R,k}] + e_{x_N}^T Q_N e_{x_N}$ with (semi-)positive definite weighting matrices Q_k and R_k . After linearising the system to $\delta x_{k+1} = A_k \delta x_k + B_k \delta u_k$, the discrete Riccati equation for non-constant A_k and B_k is applied to calculate K_k [1]. Equation (1) is evaluated backwards in time, the initial value is $P_N = Q_N$, and after that K_k as defined in (2) is calculated.

$$P_k = A_k^T P_{k+1} A_k - A_k^T P_{k+1} B_k (B_k^T P_{k+1} B_k + R_k)^{-1} B_k^T P_{k+1} A_k + Q_k \quad (1)$$

$$K_k = (B_k^T P_{k+1} B_k + R_k)^{-1} B_k^T P_{k+1} A_k \quad (2)$$

The described algorithm is applied to several full- and under-actuated systems, for example the under-actuated double pendulum on a cart. In Table 1, the configuration, momentum and actuation vectors are given, a schematic diagram is presented in Figure 2. The comparison of the Riccati-control algorithm with different coordinate choices is done for an optimal upswing from $\theta_1^0 = \theta_2^0 = \pi$ to $\theta_1^N = \theta_2^N = 0$ with $x_0^0 = x_0^N = 0$ calculated in DMOC. The simulation time is $T = 2s$, the time step is $\Delta t = 0.002s$ and the disturbed initial condition is $\theta_1 = \theta_2 = \pi - 0.1$. The controlled trajectories of all three implementations are very similar compared to each other, the qualitative behaviour is plotted

Table 1: Discrete Euler-Lagrange equations in the different choices of coordinates for the under-actuated double pendulum on a cart coordinate discrete equations of motion in "pq-formulation"

		q	p
minimal	$0 = p_k + \frac{\partial L_d(q_k, q_{k+1})}{\partial q_k} + F_d^-(q_k, q_{k+1}, u_k)$ $p_{k+1} = \frac{\partial L_d(q_k, q_{k+1})}{\partial q_{k+1}} + F_d^+(q_k, q_{k+1}, u_k)$	$\begin{bmatrix} x_0 \\ \theta_1 \\ \theta_2 \end{bmatrix}$	$\begin{bmatrix} p_{x_0} \\ p_{\theta_1} \\ p_{\theta_2} \end{bmatrix}$
redundant	$0 = p_k + \frac{\partial L_d(q_k, q_{k+1})}{\partial q_k} + F_d^-(q_k, q_{k+1}, u_k) - G^T(q_k)\lambda_k \Delta t$ $0 = g(q_{k+1})$ $p_{k+1} = \frac{\partial L_d(q_k, q_{k+1})}{\partial q_{k+1}} + F_d^+(q_k, q_{k+1}, u_k)$	$\begin{bmatrix} x_0 \\ x_1 \\ y_1 \\ x_2 \\ y_2 \end{bmatrix}$	$\begin{bmatrix} p_{x_0} \\ p_{x_1} \\ p_{y_1} \\ p_{x_2} \\ p_{y_2} \end{bmatrix}$
nullspace	$0 = {}^P p_k + P^T(q_k) \frac{\partial L_d(q_k, q_{k+1})}{\partial q_k} + P^T(q_k) F_d^-(q_k, q_{k+1}, u_k)$ $0 = g(q_{k+1})$ ${}^P p_{k+1} = P^T(q_{k+1}) \frac{\partial L_d(q_k, q_{k+1})}{\partial q_{k+1}} + P^T(q_{k+1}) F_d^+(q_k, q_{k+1}, u_k)$	$\begin{bmatrix} x_0 \\ x_1 \\ y_1 \\ x_2 \\ y_2 \end{bmatrix}$	$\begin{bmatrix} p_{x_0} \\ p_{\theta_1} \\ p_{\theta_2} \end{bmatrix}$

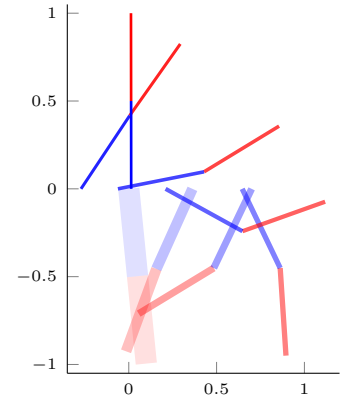


Figure 3: Perturbed upswing

in Figure 3. The blue line represents the first pendulum, the red line the second. Stepping forward in time, the lines become thinner and richer in contrast.

In Figure 4, the control effort $V_{u_k} = \sum_{i=0}^k u_{R,i}^T R_i u_{R,i}$ is plotted for all three coordinate choices. All graphs are strictly increasing as being a sum of positive terms and the gradient corresponds to the difference of the controlled trajectory to the reference trajectory. The absolute values differ between all three coordinate choices, but an adequate qualitative behaviour is ensured as cost increases occur at the same time for all three coordinate choices. After $t = 1.3s$, the perturbation is eliminated and control costs stay constant. In summary, we have implemented a Riccati feedback controller for constrained variational integrators. Both, the optimal control problem and the Riccati controller are based on the same structure preserving discrete equations of motion. With this approach, a stable handling of highly-nonlinear systems is assured.

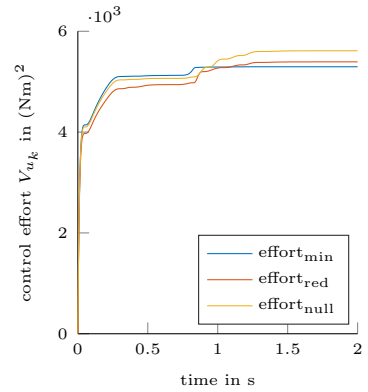


Figure 4: Control effort for perturbed upswing

By comparing the feedback control effort, it reveals that all three coordinate parametrisations only differ slightly. Thus, a different choice of coordinates can be used in the feedback control and in the optimal control problem which might be useful in practice.

References

- [1] B.D.O. Anderson and J.B. Moore. *Optimal Control: Linear Quadratic Methods*. Prentice-Hall, Inc., 1990.
- [2] E. Johnson, J.A. Schultz, and T.D. Murphey. *Structured linearization of discrete mechanical systems for analysis and optimal control*. IEEE Transactions on Automation Science and Engineering, Vol. 12, pp. 140-152, 2015.
- [3] S. Leyendecker, J.E. Marsden, and M. Ortiz. *Variational integrators for constrained dynamical systems*. ZAMM - Zeitschrift für Angewandte Mathematik und Mechanik, Vol. 88, No. 9, pp. 677-708, 2008.
- [4] S. Ober-Blöbaum, O. Junge, and J.E. Marsden. *Discrete mechanics and optimal control: An analysis*. ESAIM: COCV, Vol. 17, No. 2, pp. 322-352, 2011.

Towards higher order multi-symplectic Lie-group variational integrators for geometrically exact beam dynamics – avoidance of shear locking

Thomas Leitz, Sigrid Leyendecker

In geometrically exact beams dynamics [5], a model of slender structures is used, where the beam is represented by the position of points on the centerline and the orientation of the cross section at each point. In three-dimensional space, a point – comprised of the position and the orientation of the cross section – has six degrees of freedom, similar to a rigid body.

The derivation of higher order Lie-group variational integrators requires the interpolation of two or more points on the beam [1, 2, 4]. Doing this, special care has to be taken in order to avoid shear locking. Since shear locking is independent of the velocity, we restrict ourselves in the following to an elastostatic analysis of the beam without loss of generality.

Shear locking is a phenomenon, that arises in the formulation of the deformation energy density, which is given as

$$U(\Omega, w) = U_1(w) + U_2(\Omega) = \frac{1}{2}(w - e_3)^T C_1 (w - e_3) + \frac{1}{2}\Omega^T C_2 \Omega$$

where $w - e_3$ and Ω are the linear and angular strains, given in the material frame, and C_1 and C_2 are symmetric positive definite matrices representing the linear and angular stiffnesses of the beam. Thereby $C_1 = \text{diag}(GA, GA, EA)$ and $C_2 = \text{diag}(EI_1, EI_2, G(I_1 + I_2))$ where A is the cross section area, I_1 and I_2 are the principal area moments of inertia and E and G are Young's modulus and the shear modulus respectively. $U_1(w)$ is composed of tensile and shear energy and $U_2(\Omega)$ is composed of bending and torsional energy. For the parametrization of a point on the beam, we use $x \in \mathbb{R}^3$ for the position and a unit quaternion $p \in \mathbb{H}^1 = \{p \mid p \in \mathbb{H}, \|p\| = 1\}$ for the orientation of the cross section. The arc-length parameter $s \in [0, \ell]$ denotes the point in the undeformed configuration and the deformation map is $\varphi : s \mapsto (p, x)$. The linear strain then becomes $w - e_3 = \bar{p}x'p - e_3$, where \bar{p} is the conjugate quaternion and $x' = \frac{dx}{ds}$ is treated as a pure quaternion, i.e. the real part $\Re(x') = 0$ vanishes. The angular strain is given as $\Omega = 2\bar{p}p'$.

The beam is discretized into K elements and therefore $K + 1$ nodes. The interpolation between the nodes is done by the following method.

Interpolation The interpolation between the nodes is done using unit dual quaternions $\tilde{p} = p + \frac{\varepsilon}{2}xp$ where $\tilde{p} \in \tilde{\mathbb{H}}^1 = \{\tilde{p} \mid \tilde{p} = p_r + \varepsilon p_\varepsilon, \varepsilon^2 = 0, \|\tilde{p}\| = 1\}$ and x is treated as a pure quaternion. The interpolation is done by the normalized weighted sum of the unit dual quaternions, a.k.a dual quaternion linear blending (DLB) [3]. Therefore the positions and the orientations are interpolated at the same time. With

$$\tilde{p}(s) = \frac{\tilde{P}}{\|\tilde{P}\|} \quad \text{with} \quad \tilde{P} = \sum_{k=0}^K W_k(s) \tilde{p}_k = P_r + \varepsilon P_\varepsilon$$

the angular strain and w are

$$\Omega = \frac{2}{\|P_r\|^2} \sum_{k=0}^{K-1} \sum_{l=k+1}^K (W_k W_l' - W_l W_k') \Im(\bar{p}_k p_l)$$

$$w = \frac{1}{\|P_r\|^2} \sum_{k=0}^{K-1} \sum_{l=k+1}^K (W_k W_l' - W_l W_k') \Im[\bar{p}_k (x_l - x_k) p_l] - \frac{P_r \cdot P_\varepsilon}{\|P_r\|^2} \Omega$$

Pure bending Consider a beam – or some part of a beam – of length Δs with the following deformed configuration

$$x(s) = \frac{\Delta s}{\varphi_0} \begin{bmatrix} 1 - \cos \alpha(s) \\ 0 \\ \sin \alpha(s) \end{bmatrix} \quad w = \bar{p}x'p = \begin{bmatrix} 0 \\ 0 \\ 1 \end{bmatrix}$$

$$p(s) = \begin{bmatrix} \cos \frac{\alpha(s)}{2} \\ 0 \\ \sin \frac{\alpha(s)}{2} \end{bmatrix} \quad \Omega = 2\bar{p}p' = \begin{bmatrix} 0 \\ \frac{\varphi_0}{\Delta s} \\ 0 \end{bmatrix}$$

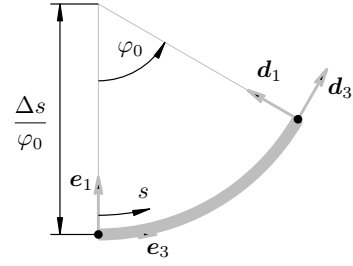


Figure 1: Pure bending

where $\alpha(s) = \frac{\varphi_0}{\Delta s}s$, i.e. the beam is bent into a circle without any elongation as depicted in Figure 1. Insertion into the deformation energy yields $U_1 = 0$ and $U_2 = \frac{1}{2}EI_2 \left(\frac{\varphi_0}{\Delta s}\right)^2$, i.e. it is only composed of bending energy. We insert the positions and orientations as x_k and p_k at α_k into the equations for the interpolated strains. The angular strain is

$$\Omega = \frac{2}{\|P\|^2} \sum_{k=0}^{K-1} \sum_{l=k+1}^K (W_k W_l' - W_l W_k') \begin{bmatrix} 0 \\ -\sin \frac{\alpha_k - \alpha_l}{2} \\ 0 \end{bmatrix}$$



Figure 2: green: without shear locking, red: with shear locking

and represents bending as expected. The linear strain is

$$w = \frac{1}{\|P_r\|^2} \frac{\Delta s}{\varphi_0} \sum_{k=1}^{K-1} \sum_{l=k+1}^K (W_k W_l' - W_l W_k') \begin{bmatrix} 0 \\ 0 \\ 2 \sin \frac{\alpha_l - \alpha_k}{2} \end{bmatrix}$$

The fact, that in w is zero in the e_1 and e_2 component is the reason why the interpolation method is free from shear locking and therefore facilitates the derivation of higher order multi-symplectic Lie-group variational integrators for geometrically exact beam dynamics without shear locking. Figure 2 shows the result of a simulation using the presented interpolation method in green, compared to the result of a simulation using a different method suffering from shear locking in red.

References

- [1] F. Demoures, F. Gay-Balmaz, M. Kobilarov, and T.S. Ratiu. *Multisymplectic Lie group variational integrator for a geometrically exact beam in R^3* . Communications in Nonlinear Science and Numerical Simulation, Vol. 19, No. 10, pp. 3492-3512, 2014.
- [2] J. Hall and M. Leok. *Lie Group Spectral Variational Integrators*. Foundations of Computational Mathematics, pp. 1-59, 2015.
- [3] L. Kavan, S. Collins, J. ra, and C.O’Sullivan. *Geometric Skinning with Approximate Dual Quaternion Blending*. ACM Trans. Graph., Vol. 27, No. 4, pp. 105:1-105:23, 2008.
- [4] T. Leitz, S. Ober-Bilbaum, and S. Leyendecker. *Variational integrators for dynamical systems with rotational degrees of freedom*. 11th World Congress on Computational Mechanics (WCCM XI), pp. 3148-3159, Barcelona, Spain, 2014.
- [5] J. Simo. *A finite strain beam formulation. The three-dimensional dynamic problem. Part I*. Computer Methods in Applied Mechanics and Engineering, Vol. 49, No. 1, pp. 55-70, 1985.

Kinematic validation of the human thumb model

Uday D. Phutane, Michael Roller¹, Staffan Björkenstam², Sigrid Leyendecker

The activity of grasping is possible due to the unique design of the human thumb and its complex movements viz. apposition, opposition etc. To simulate these complex movements, a physically correct model of the thumb is necessary. Anatomically, the thumb is made of three bones and three joints, namely the carpometacarpal (CMC) joint between the carpal (wrist) bone and the first metacarpal bone, the metacarpophalangeal (MCP) joint between the first metacarpal and the proximal phalanx bone and the interphalangeal (IP) joint between the proximal and distal phalanges.

The design of the CMC is of peculiar interest to researchers. It is a saddle joint [1] with rotations of flexion-extension (FE) and adduction-abduction (AA) and has been mathematically implemented in biomechanical models as a universal or cardan joint [2]. However, cadaver measurements [3] and more recently magnetic resonance (MR) imaging [4] have established that the CMC (and also the MCP) joints are composed with two axes of rotations which are non-orthogonal and non-intersecting, as opposed to a universal joint. Also, it has been studied that such a joint configuration is necessary to develop correct thumb tip forces in key posture and opposition posture [5].

Here, we develop a multibody model, similar to [6], of the thumb, as shown in Figure 1, with two degrees of freedom for the CMC and the MCP joints, respectively, and one degree of freedom for the IP joint. While the CMC and the MCP joints allow for motions of FE and AA, the IP joint allows only the motion of FE. The dimensions of the bones of the thumb are taken from [7] while the location and the orientation of the axes of the joints are obtained from [3].

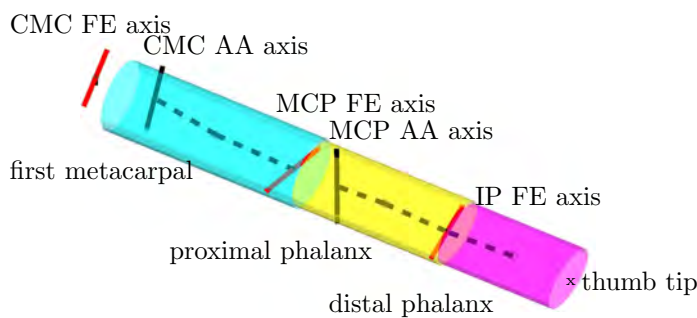


Figure 1: Thumb multibody model

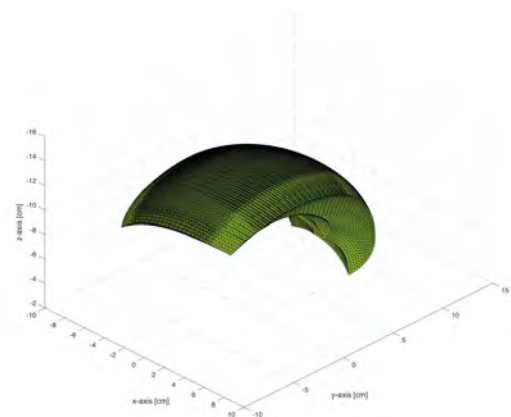


Figure 2: Point cloud of the thumb tip with maximum ROM

To validate the realistic behavior of the model, we perform a two-fold validation test. Firstly, we plot the point cloud, as shown in Figure 2, of the work-space created by the tip of the thumb by moving the thumb kinematically in all its degrees of freedom and then calculating the volume using alpha shapes. There are two sets of limits on the range of motion (ROM), namely the maximum ROM and the grasp ROM. The grasp ROM limits are smaller than the maximum ROM as grasping while performing activities of daily living is not possible with the thumb at its anatomic extreme positions. Hence, grasp ROM yields lesser volume than maximum ROM. This reduction in the volume is a kinematic measure for a thumb model. We calculate the volume reduction for the thumb model

¹Fraunhofer Institute for Industrial Mathematics, Kaiserslautern, Germany

²Fraunhofer-Chalmers Centre, Gothenburg, Sweden

we created using parameters as stated above and also for four more thumb models obtained from Monte-Carlo simulations as described in [7]. These thumb models are representative of the anatomic variability of thumb FE and AA axes in general population and have differences such as the location of the MCP FE axis being distal to the MCP AA axis in two models and vice versa in the other two models. The reduction of volume for the thumb models from our simulations is found to be in the range of 71% to 75%. We compare these values with data from literature [8], wherein the volume reduction values vary between 68% and 76%.

Secondly, we compute the axial rotation of the thumb CMC joint in different postures. The axial rotation of the thumb is an outcome from the different positions of the thumb in FE and AA as the thumb CMC does not have an active third degree of freedom to rotate around its longitudinal axis. We compare the axial rotation of the first metacarpal for different FE and AA rotations with values from literature [1]. The axial rotation resulting in our simulation lies within the limits of the standard deviation of the literature values. The results for the two validation tests are in close agreement with the literature values and consequently the thumb model can be said to have been validated kinematically.

References

- [1] W.P. Cooney, M.J. Lucca, E.Y. Chao, and R.L. Linscheid. *The kinesiology of the thumb trapeziometacarpal joint*. The Journal of Bone and Joint Surgery, Vol. 63, No. 9, pp. 1371-1381, 1981.
- [2] J.L. Sancho-Bru, M.C. Mora, B.E. León, A. Pérez-González, J.L. Iserte, and A. Morales. *Grasp modelling with a biomechanical model of the hand*. Computer methods in biomechanics and biomedical engineering, Vol. 17, No. 4, pp. 297-310, 2014.
- [3] A. Hollister, W.L. Buford, L.M. Myers, D.J. Giurintano, and A. Novick. *The axes of rotation of the thumb carpometacarpal joint*. Journal of Orthopaedic Research, Vol. 10, No. 3, pp. 454-460, 1992.
- [4] P. Cerveri, E. De Momi, M. Marchente, G. Baud-Bovy, P. Scifo, R.M.L. Barros, and G. Ferrigno. *Method for the estimation of a double hinge kinematic model for the trapeziometacarpal joint using MR imaging*. Computer methods in biomechanics and biomedical engineering, Vol. 13, No. 3, pp. 387-396, 2010.
- [5] F.J. Valero-Cuevas, M.E. Johanson, and J.D. Towles. *Towards a realistic biomechanical model of the thumb: the choice of kinematic description may be more critical than the solution method or the variability/uncertainty of musculoskeletal parameters*. Journal of biomechanics, Vol. 36, No. 7, pp. 1019-1030, 2003.
- [6] R. Maas and S. Leyendecker. *Biomechanical optimal control of human arm motion*. Journal of Multi-body Dynamics, Vol. 227, No. 4, pp. 375-389, 2013.
- [7] V.J. Santos and F.J. Valero-Cuevas. *Reported anatomical variability naturally leads to multimodal distributions of Denavit-Hartenberg parameters for the human thumb*. IEEE Transactions on Biomedical Engineering, Vol. 53, No. 2, pp. 155-163, 2006.
- [8] K. Dermitzakis, A. Ioannides, and L. Hwai-ting. *Robotic thumb grasp-based range of motion optimisation*. 35th Annual International Conference of the IEEE Engineering in Medicine and Biology Society (EMBC), pp. 3163-3166, 2013.

Time transformed mixed integer optimal control problems with impacts

Maik Ringkamp, Sina Ober-Blöbaum¹, Sigrid Leyendecker

The solutions of mixed integer optimal control problems (MIOCPs) yield optimized trajectories for dynamical systems with instantly changing dynamical behavior. The instant change is caused by a changing value of the integer valued control function $v \in \mathcal{L}^\infty(I, \mathcal{V})$ that maps the time $t \in I = [t_0, t_f]$ to an integer value $v(t) \in \mathcal{V} = \{1, 2, \dots, n_v\}$. A changing value of v leads to an instantaneously changing value of the right-hand side of the differential equation $\dot{x} = F(x, y, u, v)$. In contrast to that, slightly changing values of the control $u \in \mathcal{L}^\infty(I, \mathbb{R}^{n_u})$, the algebraic function $y \in \mathcal{L}^\infty(I, \mathbb{R}^{n_y})$ and the state function $x \in \mathcal{W}^{1,\infty}(I, \mathbb{R}^{n_x})$ lead to a slightly changing right-hand side. The direct discretization of a MIOCP leads to a mixed integer nonlinear program (MINLP) and can not be solved with gradient based optimization methods at once. We extend the work by Gerdt [1] and reformulate a MIOCP with integer dependent constraints by a time transformation to yield an ordinary optimal control problem (OCP). The time transformed MIOCP (TMIOCP) replaces the integer control function v by a fixed integer control function $\bar{v}_{N,n} \in \mathcal{L}^\infty(I, \mathcal{V})$ and introduces a time control $w \in \mathcal{L}^\infty(I, \mathbb{R})$. The time interval I is partitioned into N major intervals I_j of the length ΔI_j and n minor intervals I_j^i . The fixed integer control function $\bar{v}_{N,n}$ is defined constant on each minor interval with values $\bar{v}_{N,n}(\tau) \in \mathcal{V}$. A changing value of $w(\tau)$ for $\tau \in I_j^i$ allows to scale the length of the minor interval I_j^i , a scaling to zero deactivates the corresponding integer value $\bar{v}_{N,n}(\tau)$ and therefore allows to change the sequence of active right-hand sides F . In contrast to earlier works, we use control consistent fixed integer control functions [2] to assure that arbitrary switching is allowed in the interior of each major interval I_j . The time transformed MIOCP is shortly given in the following.

Definition 1 For a MIOCP with right-hand side $F : \mathbb{R}^{n_x} \times \mathbb{R}^{n_u} \times \mathcal{V} \rightarrow \mathbb{R}^{n_x}$, constraints $h : \mathbb{R}^{n_x} \times \mathbb{R}^{n_u} \times \mathcal{V} \rightarrow \mathbb{R}^{n_h}$, and an objective functional $J(x, u, v) = \int_I B(x, u, v) dt$ with $B : \mathbb{R}^{n_x} \times \mathbb{R}^{n_u} \times \mathcal{V} \rightarrow \mathbb{R}$ the TMIOCP reads:

$$\min_{x, u, w} \quad J^*(x, u, w) = \int_I w(\tau) B(x(\tau), u(\tau), \bar{v}_{N,n}(\tau)) d\tau \quad (1)$$

$$\text{s. t.} \quad \dot{x}(\tau) = w(\tau) F(x(\tau), y(\tau), u(\tau), \bar{v}_{N,n}(\tau)) \quad \text{for a.e. } \tau \in I \quad (2)$$

$$0 \geq w(\tau) h(x(\tau), u(\tau), \bar{v}_{N,n}(\tau)) \quad \text{for a.e. } \tau \in I \quad (3)$$

$$0 \leq w(\tau) \quad \text{for a.e. } \tau \in I \quad (4)$$

$$\Delta I_j = \int_{I_j} w(s) ds \quad \text{for } j = 1, \dots, N. \quad (5)$$

subject to possibly further path and point constraints.

In Definition 1, J^* is the time transformed objective functional and the functions B, F, h are continuously differentiable with respect to the first two arguments. The integer dependent constraints h can include algebraic constraints $g_v(x) = 0$ and further inequalities $d_v(x) \leq 0$. This allows to model systems with impacts because g_v can be used to switch holonomic constraints on or off as e.g. the fully plastic impact in the lockable double pendulum (Figure 1), for which the contact reaction force $G(q)^T \lambda$ occurs instantaneously. Impactive behavior can further be induced by non smooth controls u as in the telescope walker (Figure 2). Here, a changing integer value v can lead to an instantaneously changing control force f_v if a foot strikes the ground at the position q^{c_v} for $v = 1, \dots, 4$. To regularize the vanishing constraints (3) as in [2], the left-hand side is replaced by a value $r_1 > 0$ and the optimization is repeated, each time reusing the optimized trajectories (x_k^*, u_k^*, w_k^*) as an initial guess for the next optimization with $r_{k+1} < r_k$ until the discretized TMIOCP is finally solved for $r_{n_r} = 0$.

¹Department of Engineering Science, University of Oxford, England

The following mixed integer control systems are modeled by a forced constrained Hamiltonian with state $x = (q, p) \in \mathbb{R}^{n_x}$ and Lagrangian multiplier $y = \lambda \in \mathbb{R}^{n_y}$. Confer [3] for details on the Hamiltonian type right-hand side F and further constraint functions. In both of the presented MIOCPs the objective is the control effort $J = \frac{1}{2} \int_I u^2(t) dt$. The motion of a lockable double pendulum is optimized, resulting in the trajectories in Figure 1. Here, u represents the torque applied to the first angle q_1 . The vertical position of the first mass $-l_1 \cos(q_1)$ determines if the second angle q_2 is locked or unlocked. The optimized maneuver is a rest to rest swing up, the double pendulum starts in the downward position $q^0 = (0, 0)$ and stops in the upward position $q^f = (\frac{\pi}{2}, 0)$. The motion of the telescope walker is optimized, resulting in the trajectories in Figure 2. The optimized maneuver is an acyclic gait change from walking to running. The initial conditions are the states x^0 resulting from an optimized cyclic walking gait, moving about a distance of $0.8m$ in $t_f = 0.8s$. The final conditions are the states x^f resulting from an optimized running gait about a distance of $2.5m$ in $t_f = 0.5s$. The whole motion is restricted by a minimal height of $q_y \geq 0.7m$.

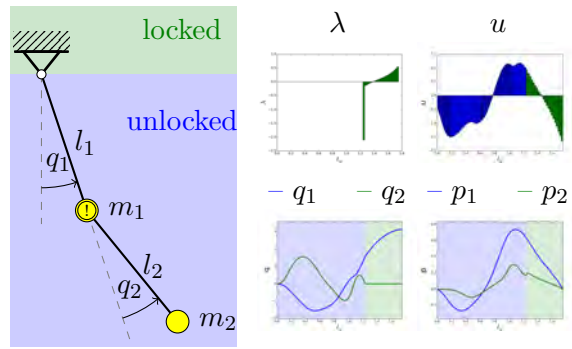


Figure 1: Sketch of the lockable double pendulum (left) with locally optimal trajectories (middle and right)

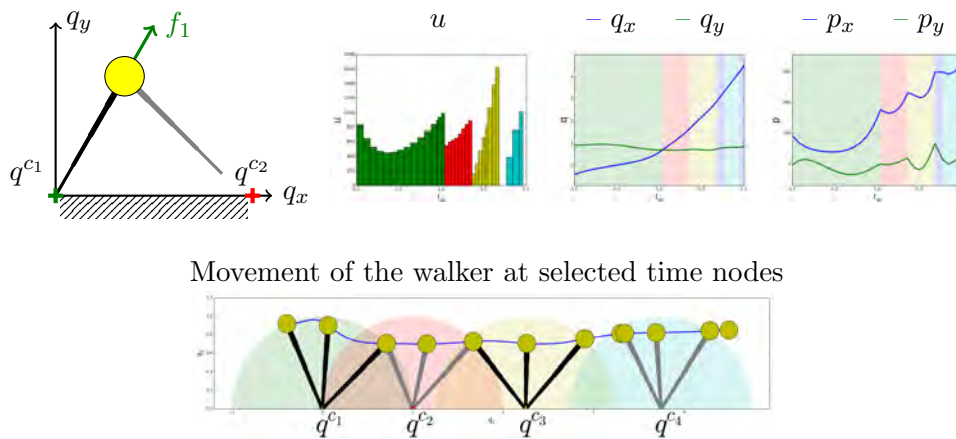


Figure 2: Sketch of the telescope walker (upper left) with locally optimal trajectories of the gait change from walking (stance phase, stance phase, ...) until q^{c3} to running (stance phase, flight phase, ...) beginning at q^{c3}

References

[1] M. Gerdt. *A variable time transformation method for mixed-integer optimal control problems*. Optimal Control Applications and Methods, Vol. 27, No. 3, pp. 169-182, 2006.

[2] M. Ringkamp, S. Ober-Blöbaum, and S. Leyendecker. *On the time transformation of mixed integer optimal control problems using a consistent fixed integer control function*. Mathematical Programming, 1-31 (2016).

[3] M. Ringkamp, S. Ober-Blöbaum, and S. Leyendecker. *Time transformed mixed integer optimal control problems with impacts*. PAMM, Vol. 16, pp. 789-790, GAMM Annual Meeting, Braunschweig, Germany, 7-11 March 2016.

Comparison of finite element models for dielectric elastomers concerning volumetric locking

Tristan Schlögl, Sigrid Leyendecker

The mechanical properties of commonly used polymers for dielectric elastomers are well covered by hyperelastic material models, where the stress-strain relation is derived from a strain energy function. Incompressibility is often approximated by a Poisson's ratio close to 0.5 or a very large bulk modulus. This, however, is like enforcing the incompressibility condition with a penalty method that, due to the spatial finite element discretisation, might lead to volumetric locking [1]. As a result, the material is artificially stiffened, not leading to physically meaningful simulation results. In analogy to the three-field formulation for pure mechanical problems [1], in this work additional degrees of freedom are added to the electromechanically coupled material model [2], leading to a multi-field formulation. Combined with reduced spatial integration for the additional fields, also known as the mean dilatation method, volume locking for incompressible and nearly incompressible materials is avoided [3]. Depending on the specific choice of additional fields, different formulations are obtained. In the framework of dielectric elastomer actuator simulation and structure preserving time integration, these formulations are compared in terms of achievable incompressibility, tendency to volume-locking and computational cost.

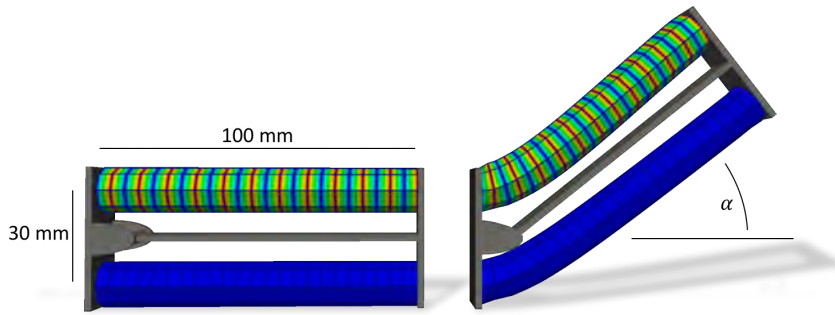


Figure 1: Revolute joint that is actuated by two artificial muscles in agonist/antagonist configuration

Four Neo-Hookean material models are investigated, each model is tested with numerical examples that are typical for dielectric actuator simulations. An example set-up is illustrated in Figure 1. All material models are based on the free energy density function Ω that is split into an isochoric term Ω_{iso} , a volumetric term Ω_{vol} and an electromechanically coupling term Ω_{elec} , such that

$$\Omega = \Omega_{\text{iso}} + \Omega_{\text{vol}} + \Omega_{\text{elec}}. \quad (1)$$

The isochoric and coupling term contributions are the same for all simulations and taken from [4]. The four different materials models differ in their volumetric part that in each case is given as

$$\Omega_{\text{vol}}^{\text{I}} = \frac{1}{2}\kappa (J - 1)^2 \quad (2a)$$

$$\Omega_{\text{vol}}^{\text{II}} = \frac{1}{2}\kappa (\bar{J} - 1)^2 + p(J - \bar{J}) \quad (2b)$$

$$\Omega_{\text{vol}}^{\text{III}} = p(J - \bar{J}) + \lambda(\bar{J} - 1) \quad (2c)$$

$$\Omega_{\text{vol}}^{\text{IV}} = \lambda(J - 1), \quad (2d)$$

where κ is the bulk modulus and J is the determinant of the deformation gradient. During finite element assembly, the dilatation field \bar{J} , the pressure field p and the Lagrange multiplier λ are treated with a reduced integration method using shape functions with reduced order [1]. Model I is based on a classical displacement formulation, extended by electromechanical coupling terms. Model II is

formulated in analogy to a nearly incompressible three-field formulation for pure mechanical problems. Model III extends model II by another field λ accounting for incompressibility. Finally, model IV is an attempt to decrease the amount of additional fields necessary to obtain incompressible behaviour.

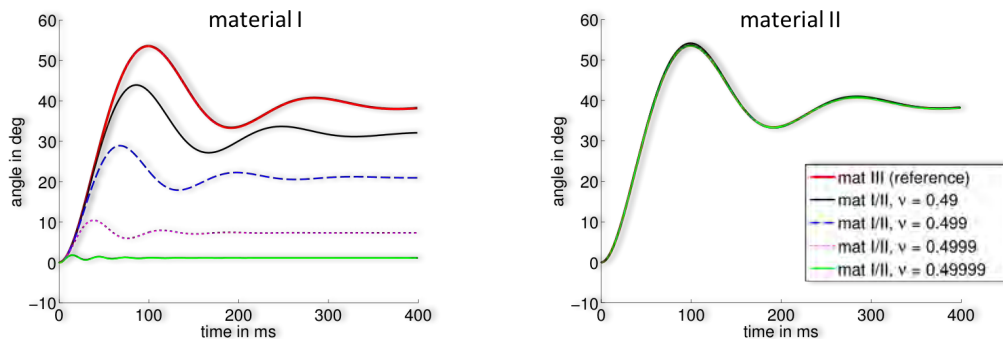


Figure 2: Transient response of the revolute joint for different material models

The transient response of the revolute joint that is controlled by two stacked actuators in agonist/antagonist configuration (see Figure 1) is simulated with all four material models. The bulk modulus $\kappa = \frac{Y}{3(1-2\nu)}$ is indirectly defined by specifying a Poisson ratio ν , where Y is the Young's modulus. The results are shown in Figure 2 and illustrate that material model I is not suited to approximate the incompressible material behaviour of dielectric elastomers. Large Poisson ratios inevitably lead to volume locking, even though the model is quite easy to implement and computationally very quick. Model II covers nearly incompressible behaviour very well in all applications, but the computational cost rises by a factor of about 2.6 compared to model I. Model III performs quite well, especially in combination with the structure preserving time integration scheme, allowing for exact incompressibility without any significant increase in computational cost. The results from model III and IV are identical to numerical accuracy. However, model IV remarkably not decreases the computational cost compared to model III and hence does not offer any notable advantages.

References

- [1] J. Bonet and R.D.Wood. *Nonlinear continuum mechanics for finite element analysis*. Cambridge University Press, 1997.
- [2] T. Schlögl and S. Leyendecker. *Dynamic simulation of dielectric elastomer actuated multibody systems*. Proceedings of the ASME 2016 Conference on Smart Materials, Adaptive Structures and Intelligent Systems, September 28-30, 2016, Stowe, VT, USA.
- [3] T. Schlögl and S. Leyendecker. *Comparison of non-locking incompressible multi-field finite element models for dielectric actuators*. International conference on Electromechanically Active Polymer (EAP) transducers & artificial muscles, June 14-15, 2016, Helsingør, Denmark.
- [4] T. Schlögl and S. Leyendecker. *Electrostatic-viscoelastic finite element model of dielectric actuators*. *Comput. Methods Appl. Mech. Engrg.*, Vol. 299, pp. 421-439, 2016.

Variational integrators of mixed order for systems acting on multiple time scales – The relation of constrained Galerkin variational integrators to Runge-Kutta methods

Theresa Wenger, Sina Ober-Blöbaum¹, Sigrid Leyendecker

Variational integrators of mixed order for systems acting on multiple time scales The simulation of mechanical systems that act on multiple time scales is challenging as a stable integration of the fast dynamics requires a highly accurate approximation whereas for the simulation of the slow part a coarser approximation is accurate enough. The presented variational integrators of mixed order couple coarse and fine approximations. We separate the unknowns q into fast q^f and slow q^s degrees of freedom. The separation now allows to use a polynomial of degree ps respectively pf to approximate the slow respectively the fast motion. Note, that only one time grid is used, with constant step size h . Furthermore, the Lagrangian of a dynamical system consists of the difference of the kinetic energy T and the potential. Assume the potential can be split in a slow part $V(q^s, q^f)$ and a fast part $W(q^f)$. Different quadrature rules with different orders are used to approximate the integral of each energy part. In particular, the Gauss and the Lobatto quadrature with orders $ordi$, $i = T, V, W$, where i corresponds to the energy integral that is approximated, are used. Requiring stationarity of the approximated action provides the variationally derived integration scheme. The conservation

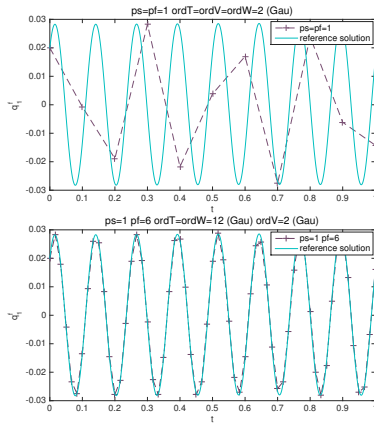


Figure 1: Simulation of q_1^f (dashed purple), reference solution (solid turquoise)

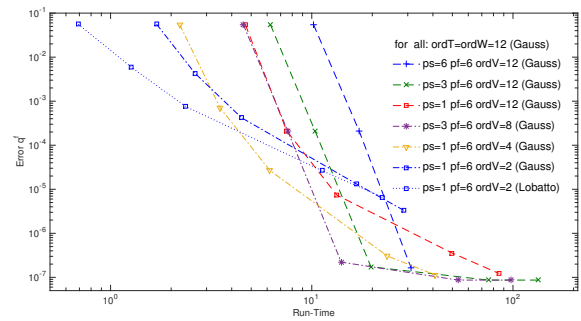


Figure 2: Global error of the fast configuration against run-time for different integrators with time steps sizes $h \in \{0.2, 0.1, 0.05, 0.01, 0.005\}$

properties, the performance and the computational efficiency of the variational integrators of mixed orders are investigated numerically by means of the FPU-problem. Fig. 1 shows the configuration of the first fast variable q_1^f (i.e. the length of the first stiff spring) calculated via the variational integrators of mixed orders with time step $h = 0.1$ (dashed lines) compared to a reference solution (solid line). In the upper plot in Fig. 1, the degree pf is one and in the lower plot, the degree pf is six whereas the degree ps of the polynomial approximating the slow configurations is in both plots one. Clearly, the fast oscillation is much better resolved, when the degree pf is high. The results of a numerical analysis regarding efficiency versus accuracy is shown in Fig. 2. It is evident that decreasing the degree of the slow polynomial from 6 (blue dashed, pluses) to 3 (green dashed, crosses) saves run-time as the number of unknowns in the discrete Euler-Lagrange equations decreases, while the accuracy suffers negligibly. In a next step we decrease the order of the quadrature formula, that approximates the slow potential, from 12 to 8 (purple dash-dotted, stars), bringing further savings in run-time while the accuracy of the solution remains nearly the same. Reducing the degree ps to 1 (red dashed line, squares) and in addition $ordV$ to 4 (yellow dash-dotted, diamonds), the savings in run-time come along with a loss in

¹Department of Engineering Science, University of Oxford, England

accuracy. In summary, assessing the efficiency of the integrators depends on the desired accuracy.

The relation of constrained Galerkin variational integrators to Runge-Kutta methods The constrained Galerkin variational integrators base on the Galerkin variational integrators, see e.g. in [2], now applied to holonomically constrained systems. Assume the motion is constrained to the constraint manifold $C = g^{-1}(0) = \{q \mid q \in \mathbb{R}^n, g(q) = 0\} \subset \mathbb{R}^n$, where $q(t) \in \mathbb{R}^n$ denotes the configuration. We use the Lagrange multiplier theorem to include the holonomic constraints $g(q)$ and consider the augmented Lagrangian \bar{L} , i.e. the Lagrangian L of a dynamical system minus the scalar product $g(q) \cdot \lambda$, where $\lambda(t)$ is the Lagrange multiplier. It is supposed that the Lagrangian is hyperregular, such that the Legendre transform $\mathbb{F}L : (q, \dot{q}) \mapsto (q, \frac{\partial L}{\partial \dot{q}}) = (q, p)$ is a global diffeomorphism with p being the conjugate momentum. A choice of finite-dimensional function spaces, approximating q via q_d of degree s respectively λ via λ_d of degree w , together with quadrature formulas is used to approximate the action. We provide sufficient conditions to ensure the solvability of the corresponding discrete Euler-Lagrange equations (DEL) and to obtain a stiffly accurate higher order integration scheme. The constrained variational integrator we focus on, has the discrete augmented Lagrangian

$$\bar{L}_d = h \sum_{i=1}^r b_i L(q_d(c_i h; q_k), \dot{q}_d(c_i h; q_k)) - h \sum_{i=0}^w e_i [g(q_d(f_i h; q_k)) \cdot \lambda_k^i] \quad (1)$$

as generating function, where $(f_i, e_i)_{i=0}^w$ are the coefficients of the Lobatto quadrature, while $(c_i, b_i)_{i=1}^r$ can be the coefficients of the Gauss or the Lobatto quadrature. The integration scheme corresponding to (1) provides a mapping of the configuration variables $C \times C \rightarrow C \times C$. The discrete conjugate momentum, calculated in a post-processing step, does not necessarily fulfill the hidden constraints $\frac{\partial g(q)}{\partial \dot{q}} \cdot \dot{q} = 0$, with $\dot{q} = (\frac{\partial L}{\partial \dot{q}})^{-1}(q, p)$. However, one can choose the representative of the equivalence class, that does fulfill the hidden constraints by applying a projection step in the post-processing. Assuming that the discrete augmented Lagrangian is self adjoint, inducing that the distribution of the polynomial control points of q_d and λ_d and the quadrature formulas are symmetric (what is true for Lobatto and Gauss quadrature), the resulting variational integrator is time reversible on configuration level. By a simple post-processing projection step, time reversibility on momentum level can be achieved. Of special interest are the constrained variational integrators with $r = s$, q_d of degree $s - 1$, $w = s - 1$ and choosing c_i , $i = 1, \dots, s$ as the control points of the Lobatto quadrature, because numerical investigations attribute them a convergence order of $2s - 2$. This indicates, that the same convergence order as for the constrained s -stage Lobatto IIIA/B method is achieved while one unknown less has to be solved for using the discrete Euler-Lagrange equations. It is well known that special classes of variational integrators are equivalent to symplectic partitioned Runge-Kutta methods, see e.g. [1]. However, when the degree of the polynomial q_d is one less than the number r of quadrature points c_i , the general Runge-Kutta construction method fails, because the internal stage derivatives $\dot{Q}_i = \dot{q}_d(c_i h)$, $i = 1, \dots, s$, become linearly dependent. A detailed analysis of the problem is given in [2], there for the unconstrained case. Furthermore, in [2] a modified Runge-Kutta method is derived that takes the linear dependence of the internal stage derivatives into account via an additional constraint. The approach given in [2] can be easily extended to the holonomically constrained case, as the internal stage derivatives \dot{Q}_i do not effect the approximation of the integral of $g(q) \cdot \lambda$.

References

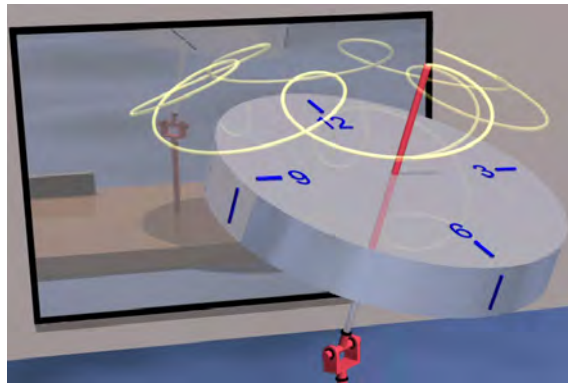
- [1] J. E. Marsden and M. West. *Discrete mechanics and variational integrators*. Acta Numerica 2001, Vol. 10, pp. 357-514, 2001.
- [2] S. Ober-Blöbaum. *Galerkin variational integrators and modified symplectic Runge-Kutta methods*. IMA Journal of Numerical Analysis, pp. 1-32, 2016.

4 Activities

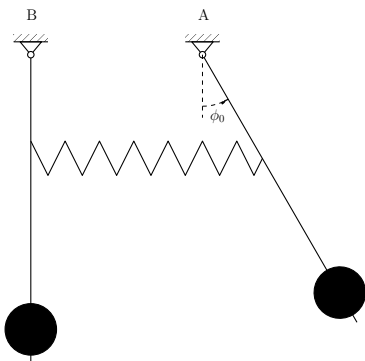
4.1 Dynamical laboratory

Dynamical laboratory – modeling, simulation and experiment The dynamical laboratory – modeling, simulation and experiment addresses all students of the Technical Faculty of the FAU Erlangen-Nuremberg. The aim of the practical course is to develop mathematical models of fundamental dynamical systems to simulate them numerically and the results are compared to measurements from the real mechanical system. Here, the students learn both the enormous possibilities of computer based modeling and its limitations. The course contains one central programming experiment and six experiments at the real existing objects, including the corresponding numerical simulation:

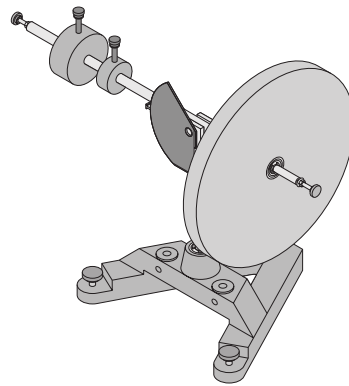
- programming training
- beating pendulums
- gyroscope
- ball balancer
- robot arm
- inverse pendulum
- balancing robot



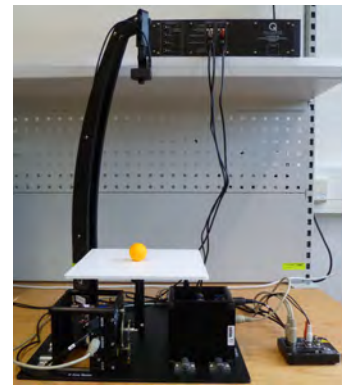
programming training



beating pendulums



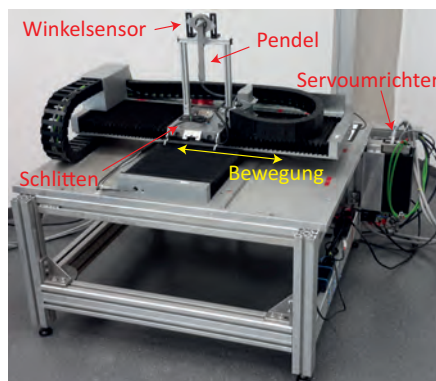
gyroscope



ball balancer



robot arm



inverse pendulum



balancing robot

Slot car racer The LTD's computer controlled slot car racer is extended by a powerful industrial camera and a new data acquisition device. The UI-3060CP USB-3 camera from IDS provides excellent image quality, a high refresh rate of 166 fps at 2.4 MP, low input delay and extremely low noise. The PCIe-6321 data acquisition board from National Instruments integrates high-performance analog, digital, and counter/timer functionality into a single device, making it well-suited to control the slot car via computer. These new components will bring significant improvement to the slot car tracking lag and hence to the control system that allows to correct the vehicle towards the desired state.



The slot car racer with the new industrial camera

4.2 Teaching

Wintersemester 2016/2017

Biomechanik der Bewegung (MT)
Vorlesung + Übung

H. Lang

Dynamik starrer Körper (MB, ME, WING, IP, BPT, CE)
Vorlesung
Übung + Tutorium

S. Leyendecker
D. Budday, D. Glaas
T. Leitz, M. Ringkamp
U. Phutane, T. Schlögl

Mehrkörperdynamik (MB, ME, WING, TM, BPT, MT)
Vorlesung
Übung

S. Leyendecker
T. Wenger

Numerische Methoden in der Mechanik (MB, ME, WING, TM, BPT, MT)
Vorlesung + Übung

H. Lang

Theoretische Dynamik II (MB, ME, WING, TM, BPT, CE, M, Ph, LaP)
Vorlesung + Übung

H. Lang

Dynamisches Praktikum – Modellierung, Simulation und Experiment (MB, ME, WING, IP)

S. Leyendecker
 H. Lang, D. Budday
 T. Gail, U. Phutane
 T. Leitz, M. Ringkamp
 T. Schlögl, T. Wenger

Sommersemester 2016

Biomechanik (MT)

Vorlesung + Übung
 geprüft

32 + 6 (WS 2015/2016)

H. Lang

Dynamik nichtlinearer Balken (MB, M, Ph, CE, ME, WING, IP, BPT)

Vorlesung + Übung
 geprüft

14

H. Lang, M. Ringkamp

Geometrische numerische Integration (MB, ME, WING, BPT)

Vorlesung
 Übung
 geprüft

4 + 2 (WS 2015/2016)

S. Leyendecker
 T. Wenger

Statik und Festigkeitslehre
 (BPT, CE, ME, MWT, MT)

Vorlesung
 Übung + Tutorium
 geprüft

457 + 525 (WS 2015/2016)

S. Leyendecker
 D. Budday, T. Gail
 D. Glaas, T. Leitz
 U. Phutane, M. Ringkamp
 T. Wenger

Theoretische Dynamik
 (TM, MB, ME, BPT, WING)

Vorlesung + Übung
 geprüft

28

H. Lang, R. Hoffmann

Rechnerunterstützte Produktentwicklung (RPE)

Versuch 6: Mehrkörpersimulation in Simulink

(MB, ME, WING) Praktikum
 Teilnehmer

60

D. Budday, T. Gail
 D. Glaas, R. Hoffmann
 T. Leitz, U. Phutane
 M. Ringkamp, T. Schlögl
 T. Wenger

Additional exams

Numerische Methoden in der Mechanik

geprüft

1

Wintersemester 2015/2016

Biomechanik der Bewegung (MT)			
Vorlesung + Übung			H. Lang
geprüft	32 + 5 (SS 2016)		
Dynamik starrer Körper (MB, ME, WING, IP, BPT, CE, MT)			
Vorlesung			H. Lang
Übung + Tutorium			D. Budday, D. Glaas
geprüft	384 + 171 (SS 2016)		T. Leitz, M. Ringkamp T. Schlögl, T. Wenger
Mehrkörperdynamik (MB, ME, WING, TM, BPT, MT)			
Vorlesung			H. Lang
Übung			T. Wenger
geprüft	63 + 9 (SS 2016)		
Dynamisches Praktikum – Modellierung, Simulation und Experiment (MB, ME, WING, IP, BPT)			
Teilnehmer	11		S. Leyendecker
			H. Lang
			D. Budday, D. Glaas
			T. Leitz, M. Ringkamp
			T. Schlögl, T. Wenger
Additional exams			
Theoretische Dynamik II			
geprüft	3		

4.3 Theses**Master theses**

- Markus Eisentraudt
Optimalsteuerung und Simulation für Systeme mit holonomen und nichtholonomen Zwangsbedingungen auf variationeller Basis
- Alexander Hetzner
On the Solution of the Karush-Kuhn-Tucker Conditions in Discrete Mechanics and Optimal Control for constrained Systems
- Murad Muradi
Entwicklung und strukturerhaltende Simulation eines autonomen PVC-Verstrichs
- Johann Penner
Modellbildung zur Optimalsteuerung einer spurgebundenen Modellrennbahn
- Roland Purucker
Bestimmung von Materialeigenschaften dielektrischer Elastomerstapelaktoren auf Silikonbasis

Project theses

- Kilian Kleeberger
Sensorintegration und Lokalisierung eines balancierenden NXT Roboters
- Sebastian Rast
2D simulation of a trapeze athlete using discrete mechanics and optimal control

Bachelor theses

- Juliane Full
Kinetische Untersuchung von Sekundärelementen in Proteinen am Beispiel von Cyclopilin A
- Michèle Gleser
Kinematik, inverse Kinematik, Dynamik und inverse Dynamik am Beispiel biomechanischer Armmodelle
- Daniel Greißel
Modellbildung und Simulation zweier gekoppelter Pendel
- Sebastian Scheiterer
Optimal control of the swing-up of an inverted pendulum

4.4 Seminar for mechanics

together with the Chair of Applied Mechanics LTM

- 04.03.2016 Daniel Greißel
Bachelor thesis, Chair of Applied Dynamics, University of Erlangen-Nuremberg
Modellbildung und Simulation zweier gekoppelter Pendel
- 18.03.2016 Staffan Björkenstam
Fraunhofer Chalmers Research Centre Industrial Mathematics, Robotics, Optimization,
Control Theory, Gothenburg, Sweden
Simulation of a balancing humanoid with non-smooth contact and feedback control
- 26.04.2016 Alexander Hetzner
Master thesis, Chair of Applied Dynamics, University of Erlangen-Nuremberg
On the solution of the Karush-Kuhn-Tucker conditions in discrete mechanics and optimal control for constrained systems
- 03.05.2016 Michele Gleser
Bachelor thesis, Chair of Applied Dynamics, University of Erlangen-Nuremberg
Kinematik, inverse Kinematik, Dynamik und inverse Dynamik für Armmodelle in der Biomechanik
- 03.05.2016 Sebastian Scheiterer
Bachelor thesis, Chair of Applied Dynamics, University of Erlangen-Nuremberg
Optimal control and practical implementation to swing up the inverted pendulum

- 05.07.2016 Juliane Full
Bachelor thesis, Chair of Applied Dynamics, University of Erlangen-Nuremberg
Kinetische Untersuchung von Sekundärelementen in Proteinen am Beispiel von Cyclopilin A
- 05.07.2016 Kilian Kleeberger
Project thesis, Chair of Applied Dynamics, University of Erlangen-Nuremberg
Sensorintegration und Lokalisierung eines balancierenden NXT Roboters
- 27.07.2016 Markus Eisentraudt
Master thesis, Chair of Applied Dynamics, University of Erlangen-Nuremberg
Optimalsteuerung und Simulation für Systeme mit holonomen und nichtholonomen Zwangsbedingungen auf variationeller Basis
- 27.07.2016 Murad Muradi
Master thesis, Chair of Applied Dynamics, University of Erlangen-Nuremberg
Entwicklung und strukturerhaltene Simulation eines autonomen PVC-Verstrichs
- 29.07.2016 Minh Tuan Duong
Department of Machine Tools and Tribology, School of Mechanical Engineering, Hanoi University of Science and Technology, Vietnam
Biomechanical Models of Soft Tissues and the Smoothed FEM
- 10.10.2016 Karin Gruber
MTI Mittelrhein, Institut für Medizintechnik und Informationsverarbeitung, Universität Koblenz-Landau, Germany
Computermodellierung individueller Wirbelsäulen mit Anwendung in der Medizin
- 18.11.2016 Gabriele Bleser and Bertram Taetz
Junior Research Group wearHEALTH, University of Kaiserslautern, Germany
Mobile motion analysis based on inertial measurement units applications, models and methods
- 22.11.2016 Johann Penner
Master thesis, Chair of Applied Dynamics, University of Erlangen-Nuremberg
Modellbildung zur Optimalsteuerung einer spurgebundenen Modellrennbahn
- 09.12.2016 Roland Purucker
Master thesis, Chair of Applied Dynamics, University of Erlangen-Nuremberg
Bestimmung von Materialeigenschaften dielektrischer Elastomerstapelaktoren auf Silikonbasis
- 09.12.2016 Sebastian Rast
Project thesis, Chair of Applied Dynamics, University of Erlangen-Nuremberg
2D simulation of a trapeze athlete using discrete mechanics and optimal control

4.5 Editorial activities

Advisory and editorial board memberships Since January 2014, Sigrid Leyendecker is a member of the advisory board of the scientific journal *Multibody System Dynamics*, Springer. She is a member of the Editorial Board of *ZAMM – Journal of Applied Mathematics and Mechanics / Zeitschrift für Angewandte Mathematik und Mechanik* since January 2016.

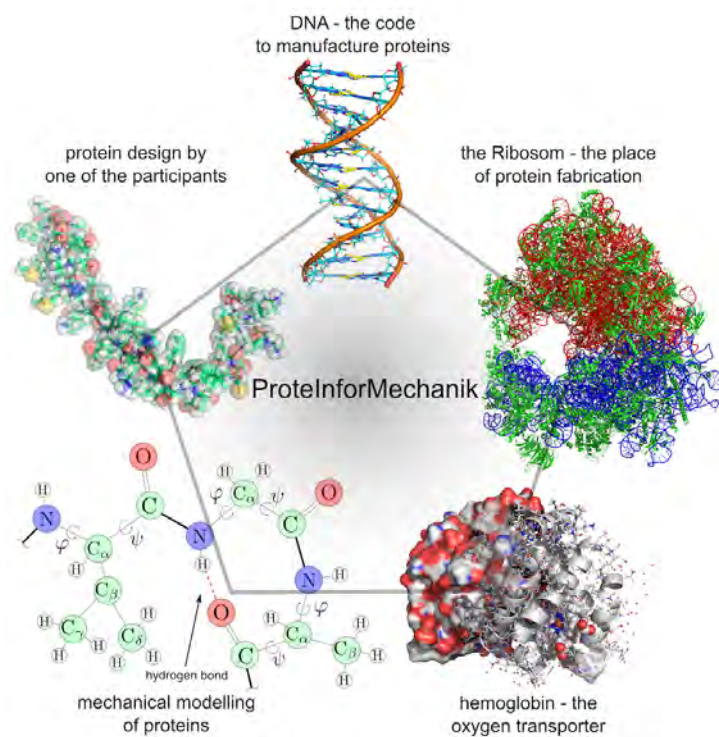
4.6 Open day – 50 years Technical Faculty of the FAU Erlangen-Nuremberg

On November 5, 2016, the Faculty of Technology of FAU celebrated its 50th anniversary. On this occasion, the university held an 'Open Day' with guided tours, lectures, and participatory activities. The Chair of Applied Dynamics participated and showed interesting experiments in its laboratories, such as the beating phenomenon for pendulums, the conservation of angular momentum, optimal control for an inverted pendulum and a Carrera race course. People had the chance to execute most of the mechanical experiments on their own, e.g. to feel forces, torques, angular velocity and acceleration experienced on a chair. Some exhibits were well suited for children such as to try to 'invert' a pendulum simply by controlling with a joystick without the help of numerical control algorithms. The atmosphere was very nice and the resonance extremely positive.



4.7 'MINT Forscherwerkstatt' 2016 with the START-Foundation

The 'MINT-Forscherwerkstatt' 2016 of the START-Foundation (in cooperation with the Deutsche Telekom-Foundation), which supports middle and high-school students with a migrational and often socially underprivileged background, took place in October 2016. Dominik Budday, who is a scholar with the Deutsch Telekom Stiftung, engaged in the research workshop as one of the group leaders, offering the course 'ProteInforMechanik' together with a fellow scholar Florian Hertrampf. Twelve participants from classes 10-12 had the chance to learn about different methods and software-tools to model and analyze the structure and function of proteins and other macromolecules. The diverse course linked various topics from high-school STEM subjects and far beyond, closely related to Dominik Buddays current research at the LTD. The strong engagement and great feedback from all participants were indicators of a successful science workshop, such that the course material shall be employed again at similar events like 'Girls Day' at the LTD.



5 Publications

5.1 Book chapters

1. M.W. Koch and S. Leyendecker. *Structure preserving optimal control of a three-dimensional upright gait*. In: M.J. Font-Llagunes (ed.) *Multibody Dynamics: Computational Methods and Applications*, Vol. 42, pp. 115-146, Springer, 2016.

5.2 Reviewed journal publications

1. M. Ringkamp, S. Ober-Blöbaum, and S. Leyendecker. *On the time transformation of mixed integer optimal control problems using a consistent fixed integer control function*. *Mathematical Programming*, pp. 1-31, 2016.
2. T. Schlögl and S. Leyendecker. *Electrostatic-viscoelastic finite element model of dielectric actuators*. *Comput. Methods Appl. Mech. Engng.*, Vol. 299, pp. 421-439, 2016.
3. M.W. Koch, M. Ringkamp, and S. Leyendecker. *Discrete Mechanics and Optimal Control (DMOCC) of Walking Gaits*. *Journal of Computational and Nonlinear Dynamics*, DOI 10.1115/1.4035213, accepted for publication, 2016.

5.3 Reviewed proceeding publications

1. H. Lang and S. Leyendecker. *Complex frequency response for linear beams with Kelvin-Voigt viscoelastic material*. In *Proceedings of the 4th Joint International Conference on Multibody System Dynamics*, 20 pages, Montreal, Canada, 29 May - 2 June 2016.
2. T. Wenger, S. Ober-Blöbaum, and S. Leyendecker. *Variational integrators of mixed order for dynamical systems with multiple time scales and split potentials*. In *Proceedings of the VII European Congress on Computational Methods in Applied Sciences and Engineering, ECCOMAS Congress*, 14 pages, Crete Island, Greece, 5-10 June 2016.
3. T. Wenger, S. Ober-Blöbaum, and S. Leyendecker. *Constrained Galerkin variational integrators and modified constrained symplectic Runge-Kutta methods*. In *Proceedings of the international Conference of Numerical Analysis and Applied Mathematics (ICNAAM)*, 4 pages, Rhodes, Greece, 19-25 September 2016.
4. T. Schlögl and S. Leyendecker. *Dynamic simulation of dielectric elastomer actuated multibody systems*. In *Proceedings of the ASME 2016 Conference on Smart Materials, Adaptive Structures and Intelligent Systems (SMASIS)*, Student Best Paper Award, 10 pages, Stowe, VT, USA, 28-30 September 2016.

5.4 Talks

1. T. Gail, S. Leyendecker, and S. Ober-Blöbaum. *Variational multirate integration in multi-body dynamics*. *GAMM Annual Meeting*, Braunschweig, Germany, 7-11 March 2016.
2. D. Glaas and S. Leyendecker. *Optimal feedback control for constrained mechanical systems*. *GAMM Annual Meeting*, Braunschweig, Germany, 7-11 March 2016.
3. R. Hoffmann, B. Taetz, M. Miezal, G. Bleser, and S. Leyendecker. *On data-guided optimal control simulation of human motion*. *GAMM Annual Meeting*, Braunschweig, Germany, 7-11 March 2016.

4. T. Leitz and S. Leyendecker. *Multisymplectic variational (Lie group) integrators for PDEs of geometrically exact beam dynamics using algorithmic differentiation*. GAMM Annual Meeting, Braunschweig, Germany, 7-11 March 2016.
5. M. Ringkamp, S. Ober-Blöbaum, and S. Leyendecker. *Time transformed mixed integer optimal control problems with impacts*. GAMM Annual Meeting, Braunschweig, Germany, 7-11 March 2016.
6. T. Wenger, S. Ober-Blöbaum, and S. Leyendecker. *Variational integrators of higher order for constrained dynamical systems*. GAMM Annual Meeting, Braunschweig, Germany, 7-11 March 2016.
7. D. Budday, R. Fonseca, S. Leyendecker, and H. van den Bedem. *Clash- and constraint guided motion planning reveals conformational transition pathways in proteins*. RECOMB, Poster, Santa Monica, California, USA, 17-21 April 2016.
8. D. Budday, S. Leyendecker, and H. van den Bedem. *Frustration-guided motion planning reveals conformational transitions in proteins*. 3DSIG, Presentation and poster, Orlando, Florida, USA, 17-21 April 2016.
9. H. Lang and S. Leyendecker. *Complex frequency response for linear beams with Kelvin-Voigt viscoelastic material*. The 4th Joint International Conference on Multibody System Dynamics, Montreal, Canada, 29 May - 2 June 2016.
10. T. Wenger, S. Ober-Blöbaum, and S. Leyendecker. *Variational integrators of mixed order for dynamical systems with multiple time scales and split potentials*. VII European Congress on Computational Methods in Applied Sciences and Engineering (ECCOMAS), Crete Island, Greece, 5-10 June 2016.
11. T. Schlögl and S. Leyendecker. *Comparison of non-locking incompressible multi-field finite element models for dielectric actuators*. EuroEAP, Poster, Helsingør, Denmark, 14-15 June, 2016.
12. D. Budday, R. Fonseca, S. Leyendecker, and H. van den Bedem. *Frustration-guided motion planning reveals conformational transitions in proteins*. Invited lecture, Donald Lab at Duke University, Durham, North Carolina, USA, 11 July 2016.
13. S. Leyendecker. *Modelling and simulation of biological and artificial muscles*. Invited lecture, International Inauguration Symposium, Muscle Research Center Erlangen (MURCE), Erlangen, Germany, 21-22 July 2016.
14. T. Wenger, S. Ober-Blöbaum, and S. Leyendecker. *Constrained Galerkin variational integrators and modified constrained symplectic Runge-Kutta methods*. International Conference of Numerical Analysis and Applied Mathematics (ICNAAM), Rhodes, Greece, 19-25 September 2016.
15. D. Budday, R. Fonseca, A. Héliou, S. Leyendecker, and H. van den Bedem. *Navigating protein conformation spaces by kino-geometric sampling and modulating frustrated motions*. Annual Meeting of the German Biophysical Society, Poster, Erlangen, Germany, 25-28 September 2016.
16. T. Schlögl and S. Leyendecker. *Dynamic simulation of dielectric elastomer actuated multibody systems*. ASME Conference on Smart Materials, Adaptive Structures and Intelligent Systems (SMASIS), Stowe, VT, USA, 28-30 September 2016.

6 Social events

Visit of the Bergkirchweih 17.05.2016



Student summer party 14.07.2016



Visit of Bamberg 22.07.2016



Christmas party together with LTM 08.12.2016





Nikolaus hike 09.12.2016

